The Atmospheric Bridge Communicated the $\delta^{13}C$ Decline during the Last Deglaciation to the Global Upper Ocean

Jun Shao[1], Lowell D. Stott[1], Laurie Menviel[2], Andy Ridgwell[3], Malin Ödalen[4,5], Mayhar Mohtadi[6]

[1]Department of Earth Science, University of Southern California, Los Angeles, CA 90089, USA
[2]Climate Change Research Centre, Earth and Sustainability Science Research Centre, University of New South Wales, NSW 2052, Sydney
[3]Department of Earth and Planetary Sciences, University of California, Riverside, CA 92521, USA
[4]Department of Meteorology, Bolin Centre for Climate Research, Stockholm University, 106 91 Stockholm, Sweden
[5]GEOMAR Helmholtz Centre for Ocean Research Kiel Duesternbrooker Weg 20 24105 Kiel, Germany
[6]MARUM-Center for Marine Environmental Sciences, University of Bremen, 28359 Germany

Correspondence to: Jun Shao (junshao@usc.edu)

Abstract. During the early part of the last glacial termination (17.2-15 ka) and coincident with a ~35ppm rise in atmospheric CO_2, a sharp 0.3-0.4‰ decline in atmospheric $\delta^{13}CO_2$ occurred, potentially constraining the key processes that account for the early deglacial CO_2 rise. A comparable $\delta^{13}C$ decline has also been documented in numerous marine proxy records from surface and thermocline-dwelling planktic foraminifera. The $\delta^{13}C$ decline recorded in planktic foraminiferal has previously been attributed to the release of respired carbon from the deep ocean that was subsequently transported within the upper ocean to sites where the signal is recorded (and then ultimately transferred to the atmosphere). Benthic $\delta^{13}C$ records from the global upper ocean, including a new record presented here from the tropical Pacific, also document this distinct early deglacial $\delta^{13}C$ decline. Here we present modeling evidence to show that rather than respired carbon from the deep ocean propagating directly to the upper ocean prior to reaching the atmosphere, the carbon would have first upwelled to the surface in the Southern Ocean where it enters the

atmosphere. In this way the transmission of isotopically light carbon to the global upper ocean was analogous to the on-going ocean invasion of fossil fuel CO_2. The model results suggest that thermocline waters throughout the ocean as well as upper-deep waters were affected by this atmospheric bridge during the early deglaciation.

1. Introduction

Atmospheric CO_2 increased by 80-100ppm between the last glacial maximum (LGM) and the Holocene (Marcott et al., 2014; Monnin et al., 2001). During the initial ~35ppm rise in CO_2 between 17.2 and 15 ka, ice core records also document a 0.3‰ contemporaneous decline in atmospheric $\delta^{13}C$ (Bauska et al., 2016; Schmitt et al., 2012) (Figure 1a, b, interval highlighted in grey). Notably, this millennial-scale trend was punctuated by an interval of even more rapid change, with a 12ppm CO_2 increase (Marcott et al., 2014) and a -0.2‰ decrease in $\delta^{13}CO_2$ (Bauska et al., 2016) occurring in an interval of just ~200 years, between 16.3-16.1 ka (Figure 1a, b, interval highlighted in red). Hypotheses proposed to explain these observations include increased Southern Ocean ventilation (e.g. Skinner et al., 2010, Burke et al., 2012), poleward shift/enhanced Southern Hemisphere westerlies (Toggweiler et al., 2006, Anderson et al., 2009, Menviel et al., 2018) and reduced iron fertilization (Martínez-García et al., 2014, Lambert et al., 2021). However, the chain of events leading to the atmospheric changes and the location(s) where the isotope signal originated is not yet well established.

Marine proxy records can provide further constraints on the possible mechanisms. For instance, during the early deglaciation, surface and thermocline dwelling foraminifera around the global ocean also recorded a distinct $\delta^{13}C$ drop (e.g. Hertzberg et al., 2016; Lund et al., 2019; Spero and Lea, 2002), an observation replicated by shallow benthic records from the tropical/subtropical

Atlantic and Indian Ocean (Lynch-Stieglitz et al., 2019; Romahn et al., 2014). These observations have often been interpreted to reflect a spread of high nutrient, low $\delta^{13}C$ waters originating in the Southern Ocean that were subsequently transported throughout the upper ocean via a so-called intermediate water teleconnection (Martínez-Botí et al., 2015; Pena et al., 2013; Spero and Lea, 2002). According to this hypothesis, formerly isolated carbon from deep waters were upwelled in the Southern Ocean (Anderson et al., 2009) in response to a breakdown of deep ocean stratification (Basak et al., 2018). This carbon was then carried by Antarctic Intermediate Water (AAIW) and Southern Ocean Mode Water (SAMW) to low latitudes where it was outgassed to the atmosphere in upwelling regions like the eastern equatorial Pacific (EEP) and recorded in ice cores. We term this scenario 'bottom up' transport, because ^{13}C-depleted carbon passes through the upper ocean globally and is recorded in marine proxy records there, before entering the atmosphere (and being recorded in ice cores). The alternative scenario to explain the early deglacial decline in planktic (and shallow benthic) $\delta^{13}C$ we term 'top down'. This recognizes the importance of air-sea exchange in conveying an isotopic signal from the atmosphere to the ocean surface rapidly (on the order of 1 yr) and globally (e.g. Schmittner et al., 2013), followed by propagation of the $\delta^{13}C$ signal from surface to upper intermediate depths occurring on a multi-decadal to centennial timescale (Heimann and Maier-Reimer 1996; Broecker et al., 1985; Eide et al., 2017). Although these timescales allow for an atmospheric $\delta^{13}C$ decline to be propagated throughout the upper ocean, this 'top down' effect has been mostly overlooked in the interpretation of marine planktic and benthic $\delta^{13}C$ records, at least until recently (Lynch-Stieglitz et al., 2019).

The 'top down' scenario has very different implications from 'bottom up'. Firstly, negative $\delta^{13}C$ excursions recorded in the upper ocean need not be associated with enhanced influx of nutrient (based on the notion that the extra nutrients came from a previously isolated deep ocean reservoir

along with isotopically depleted respired metabolic carbon). Secondly, a 'top down' scenario does not require a specific or even a single initial path of carbon to the atmosphere. Outgassing to the atmosphere could occur anywhere at the ocean surface, with a negative $\delta^{13}C$ signal that then propagates globally through air-sea gas exchange – akin to the on-going fossil fuel CO_2 emissions and the propagation of its isotopically depleted signal down through the ocean (Eide et al., 2017).

In this paper we take a two-pronged approach to help elucidate the more likely of these end-member scenarios. Firstly, we present a new benthic $\delta^{13}C$ record from the western equatorial Pacific (WEP) at 566m depth that fills an important data gap from intermediate water depths in the Pacific basin. The site is located in the pathway of SAMW and AAIW to the upper tropical Pacific (Figure 1c) and is also shallow enough be sensitive to $\delta^{13}CO_2$ changes in the 'top down' scenario. Secondly, the early deglacial section of this record is interpreted with insights gained from analyzing a transient deglacial simulation conducted with the Earth system model LOVECLIM (Menviel et al., 2018). The specific LOVECLIM simulation we utilize starts with a scenario of excess respired carbon accumulated in a more stratified deep Ocean with reduced ventilation rates. Although it is not clear if such a glacial carbon scenario is correct (Cliff et al., 2021, Stott et al., 2021), we can still make use of the ability of the model to simulate how the ocean communicates stored carbon and its isotopic composition to the atmosphere during deglaciation (the focus of this paper).

In the transient LOVECLIM simulation, sequestered respired carbon from the deep and intermediate waters is ventilated through the Southern Ocean, leading to a sharp decline in $\delta^{13}CO_2$, consistent with ice core records. We evaluate the two different $\delta^{13}C$ transport scenarios by partitioning the simulated carbon pool and its stable isotope signature into a preformed (DIC_{pref},

being the carbon that is transported passively by ocean circulation) and a respired (DIC_{soft}, being the accumulated respired carbon since the water parcel was last in contact with the atmosphere) component. Because the LOVECLIM transient experiment does not explicitly simulate either preformed or respired carbon as additional numerical tracers, the respired carbon is instead estimated by apparent oxygen utilization (AOU) – the difference between oxygen saturation and simulated [O_2] (see section 2.4). If the 'top down' transport scenario was the mechanism responsible for the $\delta^{13}C$ decline in marine proxy records from the upper 1000m depth, the preformed signal should dominate, while a regenerated signal would dominate in the 'bottom up' scenario. The carbon partitioning framework is not new - previous studies have used this framework to study the mechanisms that lead to lower glacial atmospheric CO_2 (Ito and Follows, 2005; Ödalen et al., 2018; Khatiwala et al., 2019) and processes that control $\delta^{13}CO_2$ and marine carbon isotope composition (Menviel et al., 2015; Schmittner et al., 2013). This diagnostic framework has also been applied to study the carbon cycle perturbation in response to a weaker Atlantic Meridional Overturning Circulation (AMOC) (Schmittner and Lund, 2015), albeit in experiments that were performed under constant pre-industrial conditions. However, new here is the application of a 2nd Earth System model (cGENIE (Cao et al., 2009)) to fully evaluate the AOU-based off-line approach against an explicit respired organic matter $\delta^{13}C$ tracer.

2 Methods

After describing the new foraminiferal $\delta^{13}C$ record in section 2.1, we will summarize the LOVECLIM model and published deglacial transient simulation in section 2.2. We then summarize the cGENIE earth system modelling framework and deglacial experiments in section 2.3 before describing the $\delta^{13}C$ tracer partitioning framework in section 2.4.

2.1 Stable Isotope Analyses and Age Model for Piston Core GeoB17402-2

The WEP piston core GeoB17402-2 (8°N, 126°34'E, 556m water depth) (Figure 1c) was recovered from the expedition SO-228. Planktic foraminiferal samples for ^{14}C age dating were picked from the greater than 250μm size fraction of sediment samples and were typically between 2 and 5mg. All new radiocarbon ages were measured at the University of California Irvine Accelerator laboratory. An age model (Figure S1) was developed for this core with BChron using the Marine20 calibration curve (Heaton et al., 2020) without any further reservoir age correction.

For benthic foraminiferal $\delta^{18}O$ and $\delta^{13}C$ measurements approximately 4-8 *Cibicidoides mundulus* (*C. mundulus*) were picked. These samples were cleaned by first cracking the tests open and then sonicating them in deionized water after which they were dried at low temperature. The isotope measurements were conducted at the University of Southern California on a GV Instruments Isoprime mass spectrometer equipped with an autocarb device. An in-house calcite standard (ultissima marble) was run in conjunction with foraminiferal samples to monitor analytical precision. The one standard deviation for standards measured during the study was less than 0.1‰ for both $\delta^{18}O$ and $\delta^{13}C$. The stable isotope data are reported in per mil with respect to Vienna Pee Dee Belemnite (VPDB).

2.2 LOVECLIM Deglacial Transient Simulation

The LOVECLIM model (Goosse et al., 2010) consists of a free-surface primitive equation ocean model (3° × 3°, 20 vertical levels), a dynamic–thermodynamic sea ice model, an atmospheric model based on quasi-geostrophic equations of motion (T21, three vertical levels), a land surface scheme, a dynamic global vegetation model (Brovkin et al., 1997) and a marine carbon cycle model

(Menviel et al., 2015). To study the sensitivity of the carbon cycle to different changes in oceanic circulation, a series of transient simulations of the early part of the last deglaciation (19-15ka) (Menviel et al., 2018) was performed by forcing LOVECLIM with changes in orbital parameters (Berger, 1978), changes in the freshwater surface balance as well as Northern Hemispheric ice-sheet geometry and albedo (Abe-Ouchi et al., 2007), and starting from a LGM simulation that best fit oceanic carbon isotopic (^{13}C and ^{14}C) records (Menviel et al., 2017).

The simulation we analyzed for this study is "LH1-SO-SHW" from Menviel et al, (2018). We briefly describe the applied forcing in this simulation: Firstly, a freshwater flux of 0.07 Sv is added into the North Atlantic between 17.6 ka and 16.2 ka, resulting in an AMOC shut down. Secondly, a salt flux is added into the Southern Ocean between 17.2 ka and 16.0 ka to enhance Antarctic Bottom Water (AABW) formation. Due to its relatively coarse resolution, the model could mis-represent the high southern latitude atmospheric or oceanic response to a weaker North Atlantic Deep Water (NADW). Enhanced AABW could have occurred due to a strengthening of the SH westerlies, changes in buoyancy forcing at the surface of the Southern Ocean, opening of polynyas, or sub-grid processes. Lastly, two stages of enhanced Southern Ocean westerlies are prescribed in the simulation at 17.2 ka and at 16.2 ka; this timing generally corresponds to Southern Ocean warming associated with two phases of NADW weakening during Heinrich Stadial 1 (Hodell et al., 2017). For more detail about this experiment, see Menviel et al., (2018).

We chose to focus our analysis on this particular simulation because 1) recent ice core records also suggest enhanced SO westerly winds during Heinrich stadials (Buitzert et al., 2018); 2) "LH1-SO-SHW" matches some of the important observations (e.g. ice core record of atmospheric CO_2 and $\delta^{13}CO_2$) better than the other scenarios presented in Menviel et al.,(2018); 3) the stronger SO wind

stress in "LH1-SO-SHW" leads to an increased transport of AAIW to lower latitudes, which could have impacted the intermediate depths of the global ocean.

2.3 cGENIE Simulations

The cGENIE Earth system model is based on a 3-D frictional geostrophic ocean circulation component, plus dynamic and thermodynamic sea ice components, and is configured here at a resolution of 36x36 horizontal grid with 16 vertical layers in the ocean. The configuration we employ here lacks a dynamical (GCM) atmosphere, with atmospheric transport fixed and provided via a 2-D energy-moisture balance model (Edwards and Marsh, 2005) The low-resolution ocean component and highly simplified atmospheric component make cGENIE much less computationally expensive to run than LOVECLIM. As well as facilitating multiple sensitivity experiments run to (deep ocean circulation) steady state to help partition and attribute carbon sources and pathways.

Ocean carbon storage analysis using the cGENIE model has previously utilized a range of preformed tracers, including those of phosphate (P_{pref}), dissolved inorganic carbon (DIC_{pref}), dissolved oxygen (O_{2pref}), and alkalinity (Ödalen et al., 2018). In the model, these are implemented by resetting the current value of the tracer at the ocean surface at each time-step, to the corresponding 'full' tracer, e.g. the value of DIC_{pref} is set to that of surface ocean DIC. (Technically, an anomaly is applied to each preformed tracer at the ocean surface at each time-step, equal to the difference between the current bulk tracer value and the preformed tracer value (as opposed to simply directly setting the values equal in the code). Because in the numerical scheme, all fluxes, including those induced by ocean circulation and any preformed tracer anomalies, are calculated simultaneously and only summed and applied to update the tracer concentration field at the very

end of the model time-step, preformed tracer concentrations at the ocean surface and at the end of the time-step, never exactly equal those of the bulk tracer.) Thereafter, these tracers are carried conservatively by ocean circulation, with no loss or gain due to e.g. organic matter remineralization in the ocean interior.

We expand the diagnostic tracer capabilities of cGENIE here and additionally add DIC_{soft}, which is the contribution to DIC form respired carbon. This is implemented as a tracer reset to zero at the ocean surface each time-step, but which is incremented by an amount of DIC equal to the remineralization of both particulate and dissolved organic matter and including organic carbon 'reflected' (not preserved and buried) from the sediment surface. As for the preformed tracers, ocean circulation also acts on the distribution of DIC_{soft} in the model. Figure S2 illustrates how DIC is partitioned for the preindustrial steady state of Cao et al. (2009). Note that we do not explicitly simulate DIC_{carb} (the contribution to DIC from dissolving $CaCO_3$, either in the water column or at the sediment surfce) as a 4^{th} tracer, but rather simply calculate it as the difference between DIC and $DIC_{pref} + DIC_{soft}$.

We also create a novel addition to the model – preformed and respired ^{13}C ($\delta^{13}C_{pref}$ and $\delta^{13}C_{soft}$, respectively). These are implemented as DIC_{pref} and DIC_{soft}, but for the concentrations of $DI^{13}C$. (In cGENIE, isotopes are carried explicitly as concentrations with delta (δ) values only generated in conjunction with bulk concentrations for output (and more convenient input).) Figure S3 illustrates how the $\delta^{13}C$ signature of DIC is partitioned into explicitly simulated preformed and respired carbon components, and with $\delta^{13}C_{carb}$ (the contribution to $\delta^{13}C$ of DIC from dissolved $CaCO_3$) again calculated by difference.

A full description of the cGENIE tracer scheme together with $\delta^{13}C$ tracer decomposition and attribution error analysis for both steady-state carbon cycling as well as under an idealized perturbation experiment, is available in the Supplement, with the pertinent insights summarized in Results.

Finally, we create a transient deglacial-like experiment using cGENIE, to approximately mimic some of the key features of a changing climate and carbon cycle simulated by LOVECLIM. Although AOU based errors in estimating the partitioning of respired vs. preformed $\delta^{13}C$ are already addressed via the idealized cGENIE steady-state and transient experiments (SI), decoupling in time of atmospheric CO_2 (and $\delta^{13}C$) surface climate, biological export, and the large-scale circulation of the ocean (and especially the AMOC) across the deglacial transition, may induce a mode complex evolution of AOU-based error. We address this by then calculating how the AOU-based error changes change in a deglacial-like cGENIE experiment. For this, we take a model configuration based on the idealized 'glacial' boundary conditions of Rae et al., (2020) (including increased zonal planetary albedo at high Northern Hemisphere latitudes and a 21 ka orbital configuration). The spin-up was run for 10,000 years, with prescribed atmospheric CO_2 = 278ppm, $\delta^{13}CO_2$ = -6.5‰. We then performed a transient simulation with time varying salt/freshwater flux into the North Atlantic and the Southern Ocean as well as wind stress forcing over the Southern Ocean (Figure S8). We ran this experiment with all the diagnostic tracers described above.

2.4 Separating $\delta^{13}C$ Anomalies into the Preformed ($\Delta\delta^{13}C_{pref}$) and Respired ($\Delta\delta^{13}C_{soft}$) Component

The published (Menviel et al., 2018) transient LOVECLIM model experiment that we analyze here does not include the numerical tracers required to explicitly attribute the sources of any given change in $\delta^{13}C$ in the model ocean. We hence make approximations from AOU calculated in the model experiment but assess the errors inherent in this by means of a set of experiments using a 2nd Earth system model – 'cGENIE' (Cao et al., 2009). This approach is detailed as follows (and expanded upon further in the Supplement).

We assume the following carbon isotopic mass balance:

$$\delta^{13}C * DIC = \delta^{13}C_{pref} * DIC_{pref} + \delta^{13}C_{soft} * DIC_{soft} + \delta^{13}C_{carb} * DIC_{carb} \quad (1)$$

where DIC, DIC_{pref}, DIC_{soft}, and DIC_{carb}, are the dissolved total inorganic carbon, the preformed, respired organic matter ('Csoft'), and dissolved (calcium) carbonate carbon pools, respectively. $\delta^{13}C_{pref}$, $\delta^{13}C_{soft}$, and $\delta^{13}C_{carb}$, are the corresponding isotopic signatures (as ‰) that contribute to the $\delta^{13}C$ signature of DIC and it is changes in the $\delta^{13}C$ of DIC that we assume foraminiferal records reflect.

Any given observed $\delta^{13}C$ anomaly in the ocean can then be expressed as:

$$\Delta\delta^{13}C = \Delta(\delta^{13}C_{pref} * DIC_{pref} / DIC) + \Delta(\delta^{13}C_{soft} * DIC_{soft} / DIC) + \Delta(\delta^{13}C_{carb} * DIC_{carb} / DIC) \quad (2)$$

The terms on the RHS represent the contribution of the preformed, respired, and dissolved (carbonate) components to the overall $\delta^{13}C$ change, respectively. Since the contribution of $CaCO_3$ dissolution is small in the upper 1000m (where GeoB17402-2 is located) in carbon cycle models (see also the Supplement), and since there is no ^{13}C fractionation during $CaCO_3$ formation in the LOVECLIM model, the last term on the RHS can be neglected for the purpose of this study.

We use AOU to estimate respired carbon and its contribution to the $\delta^{13}C$ changes: $\Delta(\delta^{13}C_{soft} * DIC_{soft} / DIC) = \Delta(\delta^{13}C_{soft} * AOU * R_{c:-o2} / DIC)$, where $\delta^{13}C_{soft}$ is estimated by the $\delta^{13}C$ of export POC in the overlying water column, $R_{c:-o2} = 117{:}{-}170$.

This leads to:

$$\Delta\delta^{13}C = \Delta(\delta^{13}C_{pref} * DIC_{pref} / DIC) + \Delta(\delta^{13}C_{soft} * AOU * R_{c:-o2} / DIC) \quad (3)$$

The anomaly, defined as the difference between 15 and 17.2 ka, can be expanded as:

$$\delta^{13}C^{15ka} - \delta^{13}C^{17.2ka} = \delta^{13}C_{pref}{}^{15ka} * DIC_{pref}{}^{15ka} / DIC^{15ka} - \delta^{13}C_{pref}{}^{17.2ka} * DIC_{pref}{}^{17.2ka} / DIC^{17.2ka} + \delta^{13}C_{soft}{}^{15ka} * AOU^{15ka} * R_{c:-o2} / DIC^{15ka} - \delta^{13}C_{soft}{}^{17.2ka} * AOU^{17.2ka} * R_{c:-o2} / DIC^{17.2ka} \quad (4)$$

The AOU approach to estimate respired carbon content assumes that the oxygen content of surface waters always reaches equilibrium with the overlying atmosphere. However, studies have shown that this is not always the case, particularly in water masses formed in high latitudes (Bernardello et al., 2014; Ito et al., 2004; Khatiwala et al., 2019, Cliff et al., 2021). As a result, AOU likely overestimates respired carbon content in the deep ocean. Additional errors associated with the AOU approach may result from the non-linear solubility of O_2 and respiration that does not involve O_2 consumption (i.e. through denitrification or sulphate reduction) (Shiller, 1981; Ito et al., 2004). However, to what extent these biases will affect the relative contribution of preformed and respired carbon pool on $\delta^{13}C$ anomaly in a carbon cycle perturbation event has not to our knowledge previously been evaluated. To address this, we performed a deglacial transient simulation with cGENIE (see section 2.3) and then applied equation (4) to the output, with the results then compared with the values that are explicitly simulated by cGENIE. We also conducted a simplified (modern configuration based) analysis of

steady state and transient error terms (Figure S2-S7), which we include in full in the Supplement and discuss briefly in the main text.

265

3 Results

The new GeoB17402-2 benthic $\delta^{13}C$ record from the intermediate WEP documents a -0.3 to -0.4‰ decline during the early deglaciation (Figure 1d). Although the foraminiferal $\delta^{13}C$ proxy can be complicated by temperature and carbonate ion changes (Bemis et al., 2000, Schmittner et al., 2017), and thus may not solely reflect seawater DIC $\delta^{13}C$ changes, core-top patterns of benthic foraminiferal $\delta^{13}C$ are highly correlated with present-day seawater DIC $\delta^{13}C$ (Schmittner et al., 2017). The apparent lag between the onset of decline in benthic $\delta^{13}C$ at site GeoB17402-2 (Figure 1d) and in $\delta^{13}CO_2$ appears to be due to the relatively large age model uncertainty below 154cm in the GeoB17402-2 record (median age ~16.2yr), up to 1-2 kyr (2SD) (Figure S1). Despite this age uncertainty, the new benthic record from the tropical Pacific captures a similar $\delta^{13}C$ decline as recorded from similar depth sites in the tropical/subtropical Atlantic and Indian Ocean (Lynch-Stieglitz et al., 2014, 2019; Romahn et al., 2014).

To investigate whether the early deglacial $\delta^{13}C$ decline observed at these sites in the upper ocean is dominated by the preformed or respired component, we carried out an in-depth carbon cycle analysis of the LOVECLIM transient simulation (Menviel et al., 2018). In response to the applied freshwater input to the North Atlantic (Figure 2a), the AMOC significantly weakens from its glacial state (Figure 2c). This has only a minor effect on the atmospheric CO_2 and $\delta^{13}CO_2$ (Figure 2d, 2e). In contrast, enhanced ventilation of AABW and AAIW driven by a combined freshwater (Figure 2a) and wind-stress (Figure 2b) driven breakdown of stratification leads to an atmospheric

CO_2 increase of ~25 ppm and $\delta^{13}CO_2$ decline of -0.35‰ between 17.2 and 15 ka (Figure 2d, 2e). This is a consequence of stronger upwelling bringing ^{13}C-depleted deep waters to the upper ocean with $\delta^{13}C$ generally decreasing by 0.2-0.3‰ at most locations in the upper 1000m (Figure 3a, 3d, 3g). In all sectors of the Southern Ocean below 400m, $\delta^{13}C$ increases by 0.1-0.2‰ due to stronger ventilation. Throughout the mid-depth North Atlantic, $\delta^{13}C$ decreases by more than 0.3-0.4‰ due to the AMOC weakening (Figure 3g). Finally, the stronger North Pacific deep-water formation leads to +0.3-0.4‰ $\Delta\delta^{13}C$ in the North Pacific below 1000m depth (Figure 3a).

Decomposing the LOVECLIM $\Delta\delta^{13}C$ signal into the $\Delta\delta^{13}C_{soft}$ and $\Delta\delta^{13}C_{pref}$ component, we find that the entire water column of the Southern Ocean is characterized with a strong positive $\Delta\delta^{13}C_{soft}$ (indicting a loss of respired carbon) and a strong negative $\Delta\delta^{13}C_{pref}$ (Figure 3b, 3c, 3e, 3f, 3h, 3g). In the rest of the global upper ocean (<1000m), $\Delta\delta^{13}C_{soft}$ is negative but of a magnitude smaller than 0.1‰, whereas a 0.2-0.3‰ decrease in $\Delta\delta^{13}C_{pref}$ accounts for most of the $\Delta\delta^{13}C$ signal. In the deep Indo-Pacific, $\Delta\delta^{13}C_{soft}$ and $\Delta\delta^{13}C_{pref}$ show opposite signs, with the positive $\Delta\delta^{13}C_{soft}$ dominating the net $\Delta\delta^{13}C$ (Figure 3a-3f). In the deep North Atlantic, $\Delta\delta^{13}C_{soft}$ and $\Delta\delta^{13}C_{pref}$ are both negative (Figure 3h, 3i), leading to the largest decrease in $\Delta\delta^{13}C$ across the ocean basins (Figure 3g).

For comparison, Figure 4 shows the $\Delta\delta^{13}C$, $\Delta\delta^{13}C_{soft}$ and $\Delta\delta^{13}C_{pref}$ response in a similar deglacial-like transient simulation conducted with cGENIE (see section 2.3 and Figure S8) in which the respired and preformed components are explicitly simulated. The $\Delta\delta^{13}C$ patterns (Figure 4a, 4d, 4g) are qualitatively similar with that simulated by LOVECLIM (Figure 3a, 3d, 3g), albeit the magnitude of positive $\Delta\delta^{13}C$ in the deep Pacific and negative $\Delta\delta^{13}C$ in the deep North Atlantic are larger in cGENIE (compare 3a with 4a and 3g with 4g). cGENIE does not simulate any large

positive $\Delta\delta^{13}C_{soft}$ or negative $\Delta\delta^{13}C_{pref}$ in the Southern Ocean above 3000m (Figure 4), in contrast to the AOU-based results from LOVECLIM (Figure 3). In the North Atlantic, the magnitude of negative $\Delta\delta^{13}C_{soft}$ and $\Delta\delta^{13}C_{pref}$ are both larger in cGENIE compared to LOVECLIM.

To assess the potential errors associated with the AOU-based approach we used to process the LOVECLIM output, we also calculated AOU-derived estimates of $\Delta\delta^{13}C_{soft}$ and $\Delta\delta^{13}C_{pref}$ for the cGENIE deglacial transient simulation (see section 2.4). The results suggest that throughout the mid-depth North Atlantic, the AOU-based $\Delta\delta^{13}C$ decomposition may introduce errors up to 0.3-0.4‰ under a weakening of the AMOC (Figure 5). In the Southern Ocean (south of 40°S), the AOU-based approach overestimates the magnitude of the positive $\Delta\delta^{13}C_{soft}$ and negative $\Delta\delta^{13}C_{pref}$ by 0.1-0.4‰ (Figure 5); the largest errors occur in the Pacific sector. Based on these results from cGENIE, we suggest the apparent $\Delta\delta^{13}C_{soft}$ and $\Delta\delta^{13}C_{pref}$ in the Southern Ocean shown in the LOVECLIM decomposition (Figure 3) are largely overestimated. Nonetheless, both cGENIE and LOVECLIM (after correcting the errors estimated from the cGENIE deglacial transient experiment, see Figure 5) show that the preformed component contributes -0.1 to -0.2‰ to the total $\Delta\delta^{13}C$ signal in the upper 1000m of the Southern Ocean. To the north of 40°S in the upper 1000m of the global upper ocean (except for the upper North Atlantic), the errors are relatively minor (generally much less than 0.1‰ in magnitude) and the AOU-based approach can provide a reasonably good estimate (Figure 5, also Figure S5, S7).

Finally, we further evaluate the errors inherent in the AOU-based approach to the decomposition of the different contributions to the $\delta^{13}C$ changes by means of a series of idealized steady-state and transient cGENIE experiments, described in the Supplement. From this we find that errors in estimating $\delta^{13}C_{soft}$ arise both from errors in AOU (themselves composed of errors due to assuming

air-sea equilibrium and because O_2 solubility increases nonlinearly with decreasing temperature) and from the assumption that the isotopic signature of carbon released by the remineralization of organic matter at any location in the ocean reflects that of carbon exported from the directly overlying ocean surface. The latter error turns out to be small in LOVECLIM as a consequence of its relatively small (3‰) simulated latitudinal variability in organic matter $\delta^{13}C$, leaving the better understood AOU-driven error to dominate the net uncertainty in reconstructing $\delta^{13}C_{soft}$. As a further consequence of this, under idealized transient changes in climate and ocean circulation in cGENIE (see the Supplement), the AOU-induced error in $\delta^{13}C_{soft}$ is almost invariant throughout the uppermost ca. 500 m of the ocean, simply because the error in AOU itself is close to zero here. This confirms the conclusions drawn from tracer comparisons made in deglacial cGENIE experiments that at the depth of GeoB17402-2, the AOU-based approach is relatively robust.

4 Discussion:

4.1 Atmospheric $\delta^{13}C$ Bridge

In the LOVECLIM model ^{13}C-depleted carbon is ultimately sourced from the respired carbon that accumulated in the deep and intermediate waters during the glacial period as a consequence of the imposed weakened deep-water formation (Menviel et al., 2017). We show that in this scenario the isotopic signal is first transmitted to the atmosphere through strong outgassing in the Southern Ocean (Figure 6). The atmosphere then transmits the $\delta^{13}C$ signal to the rest of the global surface and subsurface ocean through air-sea gas exchange. An illustrative example is the simulated transient $\delta^{13}C$ minimum event between 16.2 -15.8 ka in LOVECLIM (Figure 2c), which originates from the Southern Hemisphere and specifically from enhanced ventilation of AAIW (Figure 2a). In the model, if the ‘top down’ scenario is true, the upper water masses away from the Southern

Hemisphere would show similar magnitude of $\delta^{13}C_{DIC}$ changes as $\delta^{13}CO_2$. On the other hand, if the 'bottom up' scenario is true, a large negative $\delta^{13}C$ anomaly (of respired nature) should first appear in the South Pacific subtropical gyre (STGSP), as STGSP lies on the pathway between Southern Ocean water masses and those at lower latitudes. Then the signal would progressively spread to the tropics and finally reach the North Pacific. The negative $\delta^{13}C$ anomaly may also be gradually diluted along its pathway from the South Pacific to the North Pacific. However, in the LOVECLIM simulation, there is no $\delta^{13}C$ minimum in the upstream STGSP, while the atmosphere-like negative $\delta^{13}C$ anomaly appears in the EEP thermocline, the North Pacific subtropical gyre (STGNP) and North Pacific Intermediate Water (NPIW) simultaneously (Figure 7). In addition, the millennial-scale $\delta^{13}C$ evolution in these upper ocean water masses to the north of the equator exhibits a pattern of change that is similar to the atmosphere (Figure 7). The synchronized $\delta^{13}C$ changes therefore point to the dominant role of atmospheric communication rather than time-progressive oceanic transport of a low $\delta^{13}C$ signal in LOVECLIM.

In the LOVECLIM simulation, both millennial- and centennial-scale $\delta^{13}CO_2$ declines are the result of enhanced deep ocean and/or intermediate ocean ventilation originating in the Southern Ocean. Using the UVic Earth-System model, Schmittner and Lund (2015) showed that a slow-down of AMOC alone is able to weaken the global biological pump and lead to light carbon accumulation in the upper ocean and the atmosphere, without explicitly prescribing any forcing in the Southern Ocean. Despite the different prescribed forcing, $\Delta\delta^{13}C_{pref}$ also dominates the total $\Delta\delta^{13}C$ in the upper 1000m of the global ocean in the UVic experiment (See Figure 6 in Schmittner and Lund, 2015). Taken together, simulations by all three models suggest that any process that lowers $\delta^{13}CO_2$ would have an influence on the global upper ocean $\delta^{13}C$. In fact, the same phenomenon has been recurring since the beginning of the industrial era due to fossil fuel burning - known as the Suess

effect (Eide et al., 2017). The 'top down' scenario is also compatible with the concept of a nutrient teleconnection existing between the Southern Ocean and low latitudes (Palter et al., 2010; Pasquier and Holzer, 2016; Sarmiento et al., 2004). Figure 8 illustrates that stronger upwelling brings excess nutrients to the surface of the Southern Ocean. Unused nutrients are then transported to low latitudes within the upper ocean circulation (e.g. through mode waters and thermocline waters). However, a nutrient teleconnection does not, in itself, reflect an enhanced flux of ^{13}C-depleted DIC from the deep ocean to low latitudes in a 'tunnel-like' fashion (and 'bottom up' transport).

In the following sections, we present two cases where the LOVECLIM transient simulation successfully captures the early deglacial $\delta^{13}C_{DIC}$ evolution recorded in marine proxies. The model-based $\Delta\delta^{13}C$ partitioning then offers a unique opportunity to investigate the controlling mechanisms of the observed marine $\delta^{13}C$ variability. We acknowledge that there are also places where models (in both LOVECLIM and cGENIE deglacial transient simulations) fail to simulate the observed $\delta^{13}C$ trend between 17.2 and 15 ka. For instance, models simulate significant positive $\Delta\delta^{13}C$ (above 0.4-0.5‰) (Figure 3a, 4a) in the deep tropical/North Pacific whereas observations record no significant trend (Lund and Mix 1998, Stott et al., 2021). Models also simulate very small $\Delta\delta^{13}C$ (~0.1‰) in the deep tropical/northern Indian Ocean (Figure 3d, 4d) whereas proxy records document a distinct +0.3-0.4‰ trend (Waelbroeck et al., 2006, Sirocko et al., 2000). The model-data disagreement in the deep Indo-Pacific warrants future study.

4.2 Revisiting EEP Thermocline $\delta^{13}C$

Waters at EEP thermocline depths are thought to be connected to the deep ocean through AAIW from the south and NPIW from the north. The EEP is therefore a potential conduit for deep ocean carbon release to the atmosphere. On the other hand, the EEP thermocline is also shallow enough

to record an atmospheric $\delta^{13}C$ signal, either directly through gas exchange at the surface or indirectly through a preformed signal acquired from other parts of the global surface ocean. We select two EEP thermocline $\delta^{13}C$ records from different oceanographic settings (Figure 9a): site GGC17/JPC30 is near the coast, featured with relatively low surface nutrient; site ODP1238 is located in the main upwelling zone, featured with relatively high surface nutrient. Previous studies suggest the deglacial history of deep-water influence at the two sites are also distinctively different: at site ODP1238, strengthened deglacial CO_2 outgassing inferred from boron isotope data has been interpreted to reflect respired carbon transported from the Southern Ocean (Martínez-Botí et al., 2015); at site GGC17/JPC30, wood-constrained constant surface reservoir ages over the last 20 ka suggest this site was not influenced by old respired carbon from high latitudes (Zhao and Keigwin, 2018). However, the early deglacial planktic $\delta^{13}C$ records from the two sites show remarkably similar evolution, which is well captured by the LOVECLIM transient simulation (Figure 9b). By comparing Figure 3b to 3c, it is clear that the simulated $\delta^{13}C$ anomaly in the EEP thermocline (~100m) is dominated by the preformed component. The modeling evidence indicates that even though the EEP is the largest CO_2 outgassing regions (in terms of absolute ΔpCO_2, Figure S9) under an enhanced Southern Ocean upwelling scenario, its thermocline $\delta^{13}C$ is dominantly controlled by the 'top down' mechanism rather than the 'bottom up' mechanism as previously suggested (Martínez-Botí et al.,2015; Spero and Lea, 2002). The apparent conundrum can be explained by the fact that the air-sea balance of carbon isotopes is achieved through *gross* rather than *net* CO_2 exchange. Collectively, we make the case that in strong upwelling regions (e.g. the EEP) that are remotely connected to the deep ocean, thermocline $\delta^{13}C$ is still subjected to strong atmospheric overprint.

4.3 How Deep in the Ocean Can the Negative $\Delta\delta^{13}C_{pref}$ Signal from the Atmosphere Penetrate During the Early Deglaciation?

We have shown that given the dominant control of preformed $\delta^{13}C$ component in the upper ocean, some interpretations of planktic $\delta^{13}C$ records might need to be re-evaluated. Our simulations also reveal that an atmospheric influence can reach deeper than thermocline depths and down to upper intermediate depths – consistent with what Lynch-Stieglitz et al., (2019) proposed. Below 1000m, a $\Delta\delta^{13}C_{pref}$ signal from the atmosphere may still exist, but no longer dominates the total $\Delta\delta^{13}C$ as $\Delta\delta^{13}C_{soft}$ becomes increasingly important at depth. (The contribution of $\delta^{13}C_{carb}$ also increases at depth (Figure S3) and can exceed 10% of the contribution of $\delta^{13}C_{soft}$.)

It has been suggested that deglacial $\delta^{13}C$ variability in the waters above 2000m depth in the Atlantic could be driven by air-sea exchange (Lynch-Stieglitz et al., 2019). However, mid-depth (1800-2100m) benthic $\delta^{13}C$ records from the Brazil margin (~27°S) document a sharp decline of 0.4‰ at ~18 ka (Lund et al., 2019), while atmospheric $\delta^{13}CO_2$ did not decrease until ~17 ka (Bauska et al., 2016; Schmitt et al., 2012). Lund et al., (2019) argued that the early benthic $\delta^{13}C$ decline at their site seemed at odds with the idea that $\delta^{13}C_{pref}$ contributed to the early deglacial mid-depth $\delta^{13}C$ variability. The observed benthic $\delta^{13}C$ evolution between 20-15 ka at these Brazil margin sites are well simulated by LOVECLIM (Figure 10), allowing us to explore this question further. Before atmospheric $\delta^{13}CO_2$ starts to decline in LOVECLIM at ~17.2 ka, changes in $\delta^{13}C_{DIC}$ at ~2000m depth at the Brazil Margin are dominantly controlled by excess accumulation of respired carbon (indicated by highly negative $\Delta\delta^{13}C_{soft}$, Figure S10b), itself a response to the weakened AMOC, while $\Delta\delta^{13}C_{pref}$ is relatively small (Figure S10c). This is consistent with what previous studies have suggested (Lacerra et al., 2017; Lund et al., 2019; Schmittner and Lund,

2015). Interestingly, LOVECLIM also reveals a strong negative $\Delta\delta^{13}C_{pref}$ signal between 17.2 and 15 ka when atmospheric $\delta^{13}CO_2$ declines (Figure 3i). However, a positive $\Delta\delta^{13}C_{soft}$ (Figure 3h) signal originating from a loss of respired carbon due to enhanced ventilation at those depths almost completely compensates for the negative $\Delta\delta^{13}C_{pref}$, which leads to virtually no net change in $\delta^{13}C_{DIC}$ in the simulation (Figure 3g), consistent with the proxy observations (Figure 10). These results suggest that, between 17.2 and 15 ka, a negative preformed $\delta^{13}C$ signal from the atmosphere needs to be considered when interpreting benthic $\delta^{13}C$ records from the upper 2000m of the South Atlantic. The complexity associated with interpreting marine $\delta^{13}C$ records further underscores the urgent need to develop more robust means of estimating respired carbon accumulation/release from water masses.

5 Conclusions:

A transient simulation conducted by the LOVECLIM Earth system model is used as a realization of plausible pathways of low $\delta^{13}C$ signal transport under a prevailing deglacial scenario that involves Southern Ocean processes. Applying an AOU-based partitioning of carbon isotopic changes into preformed and respired components – a methodology that we scrutinize via a series of additional cGENIE Earth system model experiments – we show that ocean-atmosphere gas exchange likely dominates the negative $\delta^{13}C$ anomalies documented in global planktic and intermediate benthic $\delta^{13}C$ records between 17.2 and 15 ka. Numerical simulations further suggest that enhanced Southern Ocean upwelling can transfer $\delta^{13}C$ signals from respired carbon in the deep ocean directly to the atmosphere. Consequently, $\delta^{13}CO_2$ declines and this leaves its imprint on the rest of the global upper ocean through air-sea exchange. The preformed component dominates the upper 1000m and could account for a 0.3-0.4‰ decline in marine $\delta^{13}C$ records during the early

deglaciation, whereas the respired component becomes increasingly important at deeper depth. At the same time, the amount of upwelling in the Southern Ocean is a forcing imposed on the model rather than directly constrained. It is therefore possible there were other sites where excess carbon was ventilated to the atmosphere during the deglaciation, which would have also affected $\delta^{13}CO_2$. Our findings imply that planktic and upper intermediate benthic $\delta^{13}C$ records do not provide strong constraints on the site or the mechanisms through which CO_2 was released from the ocean to the atmosphere. Interpretations of early deglacial upper intermediate depth benthic $\delta^{13}C$ records also need to take into account an atmospheric influence. Whereas in the model simulations the source of the atmospheric signal is a direct response to enhanced Southern Ocean upwelling, our results underscore the need to find a way to fingerprint the actual source(s) of ^{13}C-depleted carbon that caused the atmospheric $\delta^{13}CO_2$ decline.

References:

Abe-Ouchi, A., Segawa, T., and Saito, F.: Climatic Conditions for modelling the Northern Hemisphere ice sheets throughout the ice age cycle, 16, 2007.

Anderson, R. F., Ali, S., Bradtmiller, L. I., Nielsen, S. H. H., Fleisher, M. Q., Anderson, B. E., and Burckle, L. H.: Wind-Driven Upwelling in the Southern Ocean and the Deglacial Rise in Atmospheric CO_2, 323, 1443–1448, https://doi.org/10.1126/science.1167441, 2009.

Basak, C., Fröllje, H., Lamy, F., Gersonde, R., Benz, V., Anderson, R. F., Molina-Kescher, M., and Pahnke, K.: Breakup of last glacial deep stratification in the South Pacific, 359, 900–904, https://doi.org/10.1126/science.aao2473, 2018.

Bauska, T. K., Baggenstos, D., Brook, E. J., Mix, A. C., Marcott, S. A., Petrenko, V. V., Schaefer, H., Severinghaus, J. P., and Lee, J. E.: Carbon isotopes characterize rapid changes in atmospheric carbon dioxide during the last deglaciation, 113, 3465–3470, https://doi.org/10.1073/pnas.1513868113, 2016.

Bemis, B. E., Spero, H. J., Lea, D. W., and Bijma, J.: Temperature influence on the carbon isotopic composition of Globigerina bulloides and Orbulina universa (planktonic foraminifera), 38, 213–228, https://doi.org/10.1016/S0377-8398(00)00006-2, 2000.

Berger, AndréL.: Long-Term Variations of Daily Insolation and Quaternary Climatic Changes, 35, 2362–2367, https://doi.org/10.1175/1520-0469(1978)035<2362:LTVODI>2.0.CO;2, 1978.

Bereiter, B., Eggleston, S., Schmitt, J., Nehrbass-Ahles, C., Stocker, T. F., Fischer, H., Kipfstuhl, S., and Chappellaz, J.: Revision of the EPICA Dome C CO_2 record from 800 to 600 kyr before present: Analytical bias in the EDC CO_2 record, 42, 542–549, https://doi.org/10.1002/2014GL061957, 2015.

Bernardello, R., Marinov, I., Palter, J. B., Sarmiento, J. L., Galbraith, E. D., and Slater, R. D.: Response of the Ocean Natural Carbon Storage to Projected Twenty-First-Century Climate Change, 27, 2033–2053, https://doi.org/10.1175/JCLI-D-13-00343.1, 2014.

Broecker, W. S., Peng, T.-H., Ostlund, G., and Stuiver, M.: The distribution of bomb radiocarbon in the ocean, J. Geophys. Res., 90, 6953, https://doi.org/10.1029/JC090iC04p06953, 1985.

Brovkin, V., Ganopolski, A., and Svirezhev, Y.: A continuous climate-vegetation classification for use in climate-biosphere studies, 101, 251–261, https://doi.org/10.1016/S0304-3800(97)00049-5, 1997.

Buizert, C., Sigl, M., Severi, M., Markle, B. R., Wettstein, J. J., McConnell, J. R., Pedro, J. B., Sodemann, H., Goto-Azuma, K., Kawamura, K., Fujita, S., Motoyama, H., Hirabayashi, M., Uemura, R., Stenni, B., Parrenin, F., He, F., Fudge, T. J., and Steig, E. J.: Abrupt ice-age shifts in southern westerly winds and Antarctic climate forced from the north, Nature, 563, 681–685, https://doi.org/10.1038/S101586-018-0727-5, 2018.

Burke, A. and Robinson, L. F.: The Southern Ocean's Role in Carbon Exchange During the Last Deglaciation, Science, 335, 557–561, https://doi.org/10.1126/science.1208163, 2012.

Cao, L., Eby, M., Ridgwell, A., Caldeira, K., Archer, D., Ishida, A., Joos, F., Matsumoto, K., Mikolajewicz, U., Mouchet, A., Orr, J. C., Plattner, G.-K., Schlitzer, R., Tokos, K., Totterdell, I., Tschumi, T., Yamanaka, Y., and Yool, A.: The role of ocean transport in the uptake of anthropogenic CO_2, 6, 375–390, https://doi.org/10.5194/bg-6-375-2009, 2009.

Cliff, E., Khatiwala, S., and Schmittner, A.: Glacial deep ocean deoxygenation driven by biologically mediated air–sea disequilibrium, Nat. Geosci., 14, 43–50, https://doi.org/10.1038/S101561-020-00667-z, 2021.

Edwards, N. R. and Marsh, R.: Uncertainties due to transport-parameter sensitivity in an efficient 3-D ocean-climate model, 24, 415–433, https://doi.org/10.1007/s00382-004-0508-8, 2005.

Eide, M., Olsen, A., Ninnemann, U. S., and Eldevik, T.: A global estimate of the full oceanic ^{13}C Suess effect since the preindustrial: Full Oceanic ^{13}C Suess Effect, Global Biogeochem. Cycles, 31, 492–514, https://doi.org/10.1002/2016GB005472, 2017.

Goosse, H., Brovkin, V., Fichefet, T., Haarsma, R., Huybrechts, P., Jongma, J., Mouchet, A., Selten, F., Barriat, P.-Y., Campin, J.-M., Deleersnijder, E., Driesschaert, E., Goelzer, H., Janssens, I., Loutre, M.-F., Morales Maqueda, M. A., Opsteegh, T., Mathieu, P.-P., Munhoven, G., Pettersson, E. J., Renssen, H., Roche, D. M., Schaeffer, M., Tartinville, B., Timmermann, A., and Weber, S. L.: Description of the Earth system model of intermediate complexity LOVECLIM version 1.2, 3, 603–633, https://doi.org/10.5194/gmd-3-603-2010, 2010.

Heaton, T. J., Köhler, P., Butzin, M., Bard, E., Reimer, R. W., Austin, W. E. N., Bronk Ramsey, C., Grootes, P. M., Hughen, K. A., Kromer, B., Reimer, P. J., Adkins, J., Burke, A., Cook, M. S., Olsen, J., and Skinner, L. C.: Marine20—The Marine Radiocarbon Age Calibration Curve (0–55,000 cal BP), Radiocarbon, 62, 779–820, https://doi.org/10.1017/RDC.2020.68, 2020.

Heimann, M. and Maier-Reimer, E.: On the relations between the oceanic uptake of CO_2 and its carbon isotopes, Global Biogeochem. Cycles, 10, 89–110, https://doi.org/10.1029/95GB03191, 1996.

Hertzberg, J. E., Lund, D. C., Schmittner, A., and Skrivanek, A. L.: Evidence for a biological pump driver of atmospheric CO_2 rise during Heinrich Stadial 1: Bio Pump and CO_2 Rise During HS1, 43, 12,242-12,251, https://doi.org/10.1002/2016GL070723, 2016.

Hodell, D. A., Nicholl, J. A., Bontognali, T. R. R., Danino, S., Dorador, J., Dowdeswell, J. A., Einsle, J., Kuhlmann, H., Martrat, B., Mleneck-Vautravers, M. J., Rodríguez-Tovar, F. J., and Röhl, U.: Anatomy of Heinrich Layer 1 and its role in the last deglaciation: HEINRICH EVENT 1, 32, 284–303, https://doi.org/10.1002/2016PA003028, 2017.

Ito, T. and Follows, M. J.: Preformed phosphate, soft tissue pump and atmospheric CO₂, 63, 813–839, https://doi.org/10.1357/0022240054663231, 2005.

Ito, T., Follows, M. J., and Boyle, E. A.: Is AOU a good measure of respiration in the oceans?: AOU AND RESPIRATION, 31, n/a-n/a, https://doi.org/10.1029/2004GL020900, 2004.

Khatiwala, S., Schmittner, A., and Muglia, J.: Air-sea disequilibrium enhances ocean carbon storage during glacial periods, 5, eaaw4981, https://doi.org/10.1126/sciadv.aaw4981, 2019.

Lacerra, M., Lund, D., Yu, J., and Schmittner, A.: Carbon storage in the mid-depth Atlantic during millennial-scale climate events: Mid-depth Atlantic Carbon Storage, 32, 780–795, https://doi.org/10.1002/2016PA003081, 2017.

Lambert, F., Opazo, N., Ridgwell, A., Winckler, G., Lamy, F., Shaffer, G., Kohfeld, K., Ohgaito, R., Albani, S., and Abe-Ouchi, A.: Regional patterns and temporal evolution of ocean iron fertilization and CO2 drawdown during the last glacial termination, Earth and Planetary Science Letters, 554, 116675, https://doi.org/10.1016/j.epsl.2020.116675, 2021.

Lund, D. C. and Mix, A. C.: Millennial-scale deep water oscillations: Reflections of the North Atlantic in the deep Pacific from 10 to 60 ka, Paleoceanography, 13, 10–19, https://doi.org/10.1029/97PA02984, 1998.

Lund, D., Hertzberg, J., and Lacerra, M.: Carbon isotope minima in the South Atlantic during the last deglaciation: evaluating the influence of air-sea gas exchange, 14, 055004, https://doi.org/10.1088/1748-9326/ab126f, 2019.

Lynch-Stieglitz, J., Valley, S. G., and Schmidt, M. W.: Temperature-dependent ocean–atmosphere equilibration of carbon isotopes in surface and intermediate waters over the deglaciation, 506, 466–475, https://doi.org/10.1016/j.epsl.2018.11.024, 2019.

Marcott, S. A., Bauska, T. K., Buizert, C., Steig, E. J., Rosen, J. L., Cuffey, K. M., Fudge, T. J., Severinghaus, J. P., Ahn, J., Kalk, M. L., McConnell, J. R., Sowers, T., Taylor, K. C., White, J. W. C., and Brook, E. J.: Centennial-scale changes in the global carbon cycle during the last deglaciation, 514, 616–619, https://doi.org/10.1038/nature13799, 2014.

Martínez-Botí, M. A., Marino, G., Foster, G. L., Ziveri, P., Henehan, M. J., Rae, J. W. B., Mortyn, P. G., and Vance, D.: Boron isotope evidence for oceanic carbon dioxide leakage during the last deglaciation, 518, 219–222, https://doi.org/10.1038/nature14155, 2015.

Martinez-Garcia, A., Sigman, D. M., Ren, H., Anderson, R. F., Straub, M., Hodell, D. A., Jaccard, S. L., Eglinton, T. I., and Haug, G. H.: Iron Fertilization of the Subantarctic Ocean During the Last Ice Age, 343, 1347–1350, https://doi.org/10.1126/science.1246848, 2014.

Menviel, L., Mouchet, A., Meissner, K. J., Joos, F., and England, M. H.: Impact of oceanic circulation changes on atmospheric $\delta^{13}CO_2$: $\delta^{13}CO_2$, 29, 1944–1961, https://doi.org/10.1002/2015GB005207, 2015.

Menviel, L., Yu, J., Joos, F., Mouchet, A., Meissner, K. J., and England, M. H.: Poorly ventilated deep ocean at the Last Glacial Maximum inferred from carbon isotopes: A data-model comparison study: LGM $\delta^{13}C$, 32, 2–17, https://doi.org/10.1002/2016PA003024, 2017.

Menviel, L., Spence, P., Yu, J., Chamberlain, M. A., Matear, R. J., Meissner, K. J., and England, M. H.: Southern Hemisphere westerlies as a driver of the early deglacial atmospheric CO_2 rise, 9, https://doi.org/10.1038/S101467-018-04876-4, 2018.

Monnin, E., Indermuhle, A., Dallenbach, A., Fluckiger, J., Stauffer, B., Stocker, T. F., Raynaud, D., and Barnola, J.-M.: Atmospheric CO_2 Concentrations over the Last Glacial Termination, 291, 112–114, https://doi.org/10.1126/science.291.5501.112, 2001.

Ödalen, M., Nycander, J., Oliver, K. I. C., Brodeau, L., and Ridgwell, A.: The influence of the ocean circulation state on ocean carbon storage and CO₂ drawdown potential in an Earth system model, 15, 1367–1393, https://doi.org/10.5194/bg-15-1367-2018, 2018.

Palter, J. B., Sarmiento, J. L., Gnanadesikan, A., Simeon, J., and Slater, R. D.: Fueling export production: nutrient return pathways from the deep ocean and their dependence on the

Meridional Overturning Circulation, 7, 3549–3568, https://doi.org/10.5194/bg-7-3549-2010, 2010.

Pasquier, B. and Holzer, M.: The plumbing of the global biological pump: Efficiency control through leaks, pathways, and time scales: PLUMBING OF THE GLOBAL BIOLOGICAL PUMP, 121, 6367–6388, https://doi.org/10.1002/2016JC011821, 2016.

Pena, L. D., Goldstein, S. L., Hemming, S. R., Jones, K. M., Calvo, E., Pelejero, C., and Cacho, I.: Rapid changes in meridional advection of Southern Ocean intermediate waters to the tropical Pacific during the last 30kyr, 368, 20–32, https://doi.org/10.1016/j.epsl.2013.02.028, 2013.

Rae, J. W. B., Gray, W. R., Wills, R. C. J., Eisenman, I., Fitzhugh, B., Fotheringham, M., Littley, E. F. M., Rafter, P. A., Rees-Owen, R., Ridgwell, A., Taylor, B., and Burke, A.: Overturning circulation, nutrient limitation, and warming in the Glacial North Pacific, 6, eabd1654, https://doi.org/10.1126/sciadv.abd1654, 2020.

Romahn, S., Mackensen, A., Groeneveld, J., and Pätzold, J.: Deglacial intermediate water reorganization: new evidence from the Indian Ocean, 10, 293–303, https://doi.org/10.5194/cp-10-293-2014, 2014.

Sarmiento, J. L., Gruber, N., Brzezinski, M. A., and Dunne, J. P.: High-latitude controls of thermocline nutrients and low latitude biological productivity, 427, 56–60, https://doi.org/10.1038/nature02127, 2004.

Schmitt, J., Schneider, R., Elsig, J., Leuenberger, D., Lourantou, A., Chappellaz, J., Kohler, P., Joos, F., Stocker, T. F., Leuenberger, M., and Fischer, H.: Carbon Isotope Constraints on the Deglacial CO_2 Rise from Ice Cores, 336, 711–714, https://doi.org/10.1126/science.1217161, 2012.

Schmittner, A. and Lund, D. C.: Early deglacial Atlantic overturning decline and its role in atmospheric CO_2 rise inferred from carbon isotopes ($\delta^{13}C$), 11, 135–152, https://doi.org/10.5194/cp-11-135-2015, 2015.

Schmittner, A., Gruber, N., Mix, A. C., Key, R. M., Tagliabue, A., and Westberry, T. K.: carbon isotope ratios (δ13C) in the ocean, 24, 2013.

Schmittner, A., Bostock, H. C., Cartapanis, O., Curry, W. B., Filipsson, H. L., Galbraith, E. D., Gottschalk, J., Herguera, J. C., Hoogakker, B., Jaccard, S. L., Lisiecki, L. E., Lund, D. C., Martínez-Méndez, G., Lynch-Stieglitz, J., Mackensen, A., Michel, E., Mix, A. C., Oppo, D. W., Peterson, C. D., Repschläger, J., Sikes, E. L., Spero, H. J., and Waelbroeck, C.: Calibration of the carbon isotope composition ($\delta^{13}C$) of benthic foraminifera, 32, 512–530, https://doi.org/10.1002/2016PA003072, 2017.

Shiller, A. M.: Calculating the oceanic CO2 increase: A need for caution, J. Geophys. Res., 86, 11083, https://doi.org/10.1029/JC086iC11p11083, 1981.

Sirocko, F.: Processes controlling trace element geochemistry of Arabian Sea sediments during the last 25,000 years, 26, 217–303, https://doi.org/10.1016/S0921-8181(00)00046-1, 2000.

Skinner, L. C., Fallon, S., Waelbroeck, C., Michel, E., and Barker, S.: Ventilation of the Deep Southern Ocean and Deglacial CO2 Rise, Science, 328, 1147–1151, https://doi.org/10.1126/science.1183627, 2010.

Spero, H. J.: The Cause of Carbon Isotope Minimum Events on Glacial Terminations, 296, 522–525, https://doi.org/10.1126/science.1069401, 2002.

Spero, H. J., Mielke, K. M., Kalve, E. M., Lea, D. W., and Pak, D. K.: Multispecies approach to reconstructing eastern equatorial Pacific thermocline hydrography during the past 360 kyr: PAST EASTERN EQUATORIAL PACIFIC HYDROGRAPHY, 18, n/a-n/a, https://doi.org/10.1029/2002PA000814, 2003.

Stott, L. D., Shao, J., Yu, J., and Harazin, K. M.: Evaluating the Glacial˜Deglacial Carbon Respiration and Ventilation Change Hypothesis as a Mechanism for Changing Atmospheric CO_2, Geophys Res Lett, 48, https://doi.org/10.1029/2020GL091296, 2021.

Toggweiler, J. R., Russell, J. L., and Carson, S. R.: Midlatitude westerlies, atmospheric CO_2 , and climate change during the ice ages: WESTERLIES AND CO $_2$ DURING THE ICE AGES, 21, n/a-n/a, https://doi.org/10.1029/2005PA001154, 2006.

Waelbroeck, C., Levi, C., Duplessy, J., Labeyrie, L., Michel, E., Cortijo, E., Bassinot, F., and Guichard, F.: Distant origin of circulation changes in the Indian Ocean during the last deglaciation, Earth and Planetary Science Letters, 243, 244–251, https://doi.org/10.1016/j.epsl.2005.12.031, 2006.

Zhao, N. and Keigwin, L. D.: An atmospheric chronology for the glacial-deglacial Eastern Equatorial Pacific, 9, https://doi.org/10.1038/S101467-018-05574-x, 2018.

Data availability. The stable isotope and radiocarbon data are archived on the National Climatic Data Center – NOAA: https://www.ncdc.noaa.gov/paleo-search/study/33094. All modeling data generated or analyzed during this study can be made available upon request to the corresponding author (J.S.).

The code for the version of the 'muffin' release of the cGENIE Earth system model used in this paper, is tagged as v0.9.24, and is assigned a DOI: 10.5281/zenodo.4903423.

Configuration files for the specific experiments presented in the paper can be found in the directory: genie-userconfigs/MS/shaoetal.2021. Details of the experiments, plus the command line needed to run each one, are given in the readme.txt file in that directory. All other configuration files and boundary conditions are provided as part of the code release.

A manual detailing code installation, basic model configuration, tutorials covering various aspects of model configuration and experimental design, plus results output and processing, is assigned a DOI: 10.5281/zenodo.4903426.

Author contribution. J.S. designed the research with input from L.S. L.M. provided the LOVECLIM output. A.R. implemented the new diagnostic tracers in cGENIE. J.S. performed the cGENIE simulations with help from A.R. J.S, L.M. and M.Ö analyzed the model simulations. M.M was the chief scientist of the SO-228 expedition and provided samples from the GeoB 17402-2 core. J.S. wrote the manuscript with contributions from all co-authors. A.R. wrote the supplemental text.

Competing interests. The authors declare that they have no conflict of interest.

Acknowledgements. This work is supported by the National Science Foundation under Grant Numbers 1558990 (to J.S. and L.S.) and 1736771 (A.R.). A.R. additionally recognizes support from the Heising Simons Foundation. L.M. acknowledges funding from the Australian Research Council grant FT180100606. The funding for the expedition SO-228 is from BMBF (German Ministry of Education and Research) grant #03G0228A. We thank Fortunat Joos and another anonymous reviewer for their constructive comments and prompting that helped to significantly improve this manuscript.

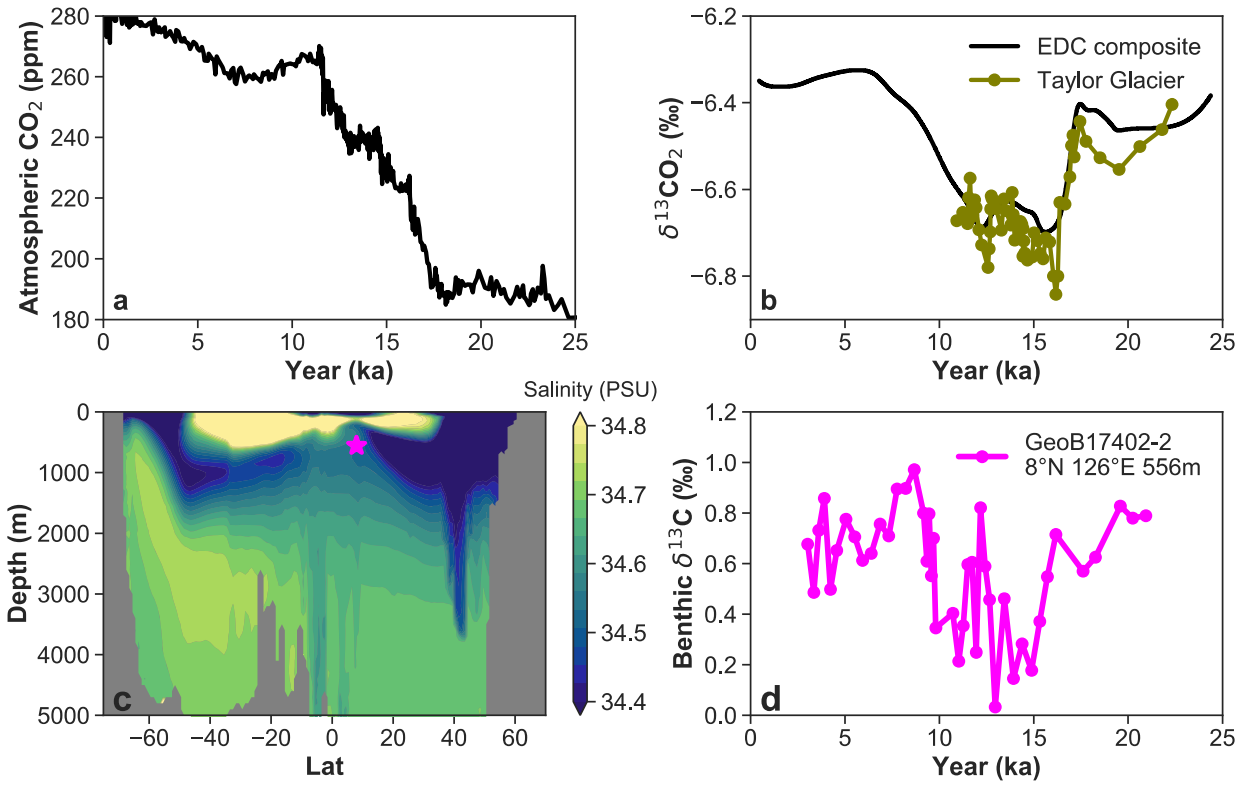

740

Figure 1. a) Ice core records of atmospheric CO_2 (Bereiter et al., 2015; Marcott et al., 2014). b) $\delta^{13}CO_2$ records (Bauska et al., 2016; Schmitt et al., 2012). c) WOA-18 Pacific zonal mean (120-160°E) salinity, the magenta star marks the GeoB17402-2 site. d) *C. mundulus* $\delta^{13}C$ record for upper intermediate depth and mode waters in the western equatorial Pacific. The

745 **millennial- and centennial-scale events in these records are highlighted in grey and red, respectively.**

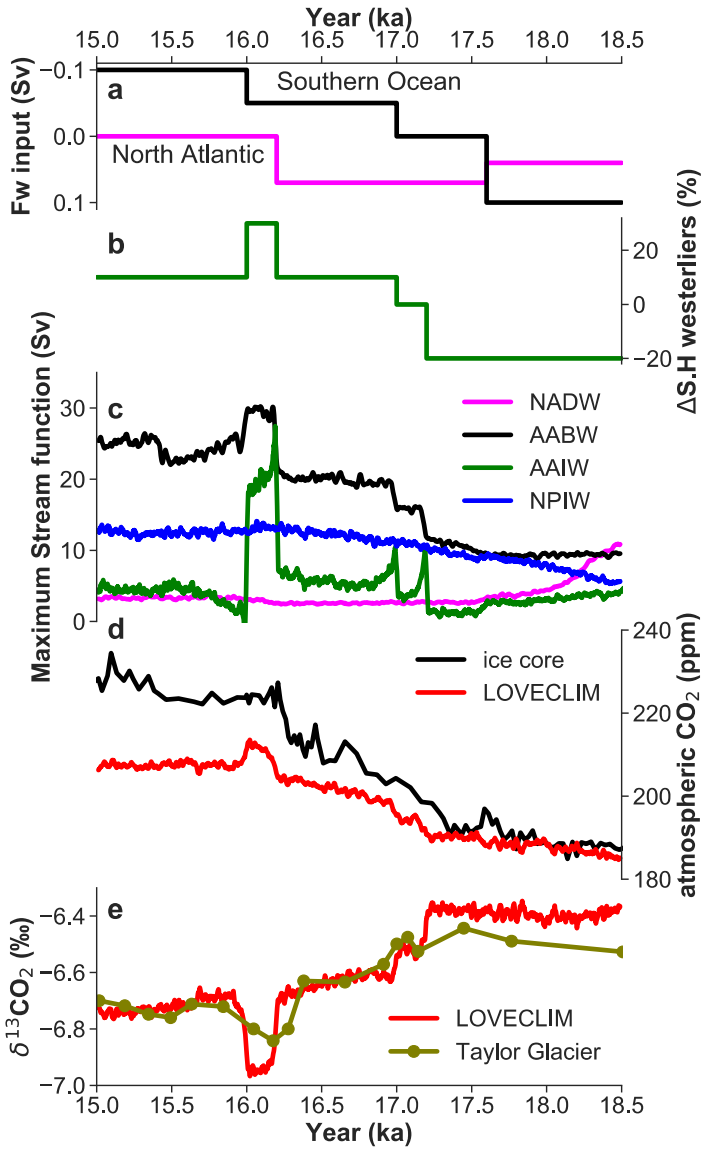

Figure 2. Timeseries from the LOVECLIM transient experiment (Menviel et al., 2018). a) Freshwater input into the North Atlantic and the Southern Ocean; b) Southern Hemisphere westerly wind forcing; c) simulated NADW, AABW, AAIW and NPIW maximum stream function in LOVECLIM. 21-year moving averages are shown for the maximum stream function to filter the high-frequency variability; d) Ice core record of atmospheric CO_2 (Bereiter et al., 2015; Marcott et al., 2014) and LOVECLIM simulated atmospheric CO_2; e) The Taylor glacier $\delta^{13}CO_2$ record (Bauska et al., 2016) and LOVECLIM simulated $\delta^{13}CO_2$.

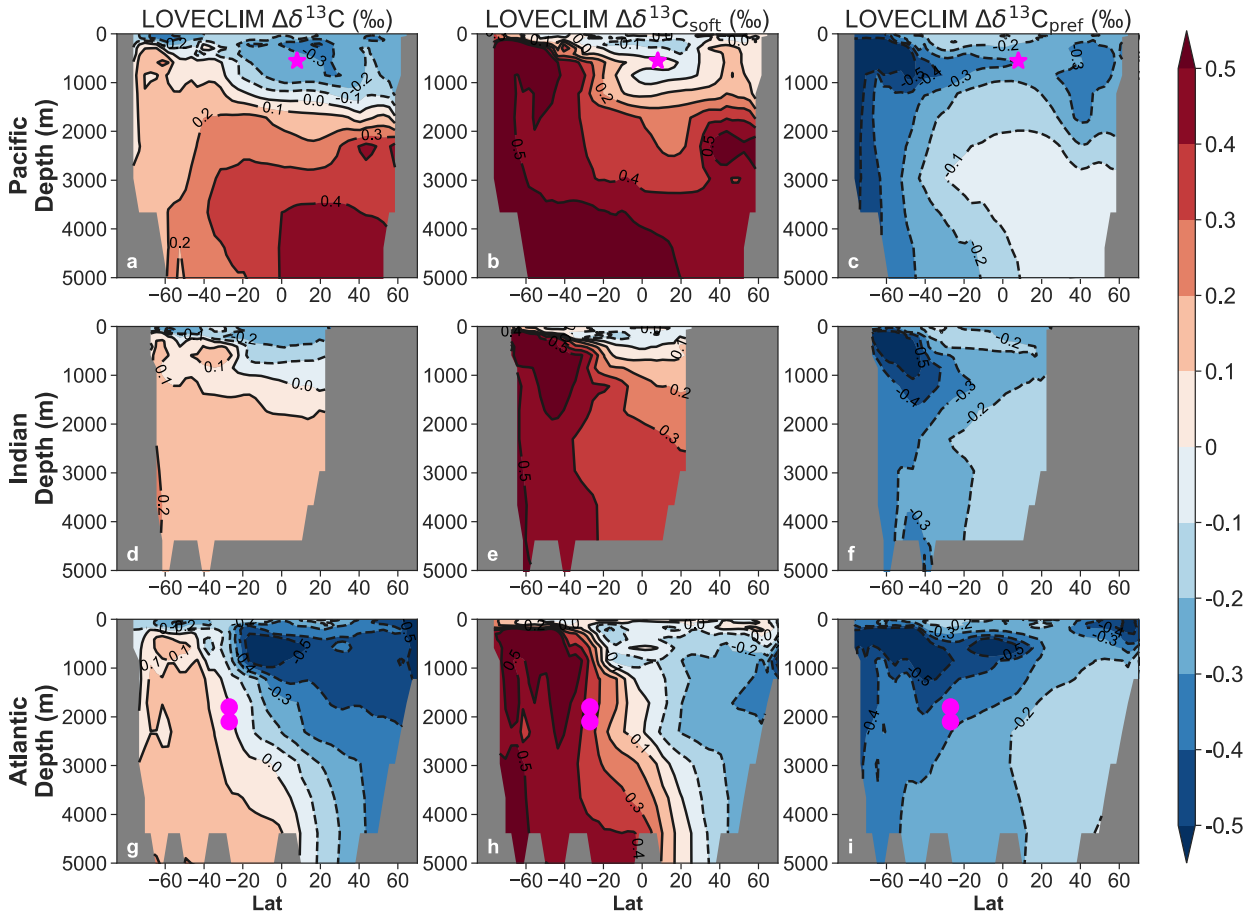

Figure 3. Ocean basin zonal mean anomalies (15ka minus 17.2ka) as simulated in LOVECLIM. Top row: Pacific zonal mean anomaly (160°E-140°W). The magenta star marks the GeoB17402-2 site. Mid row: Indian zonal mean anomaly (50-90°E). Bottom row: Atlantic zonal mean anomaly (60°W-10°W). The magenta circles mark the 78GGC and the 33GGC site discussed in section 4.3.

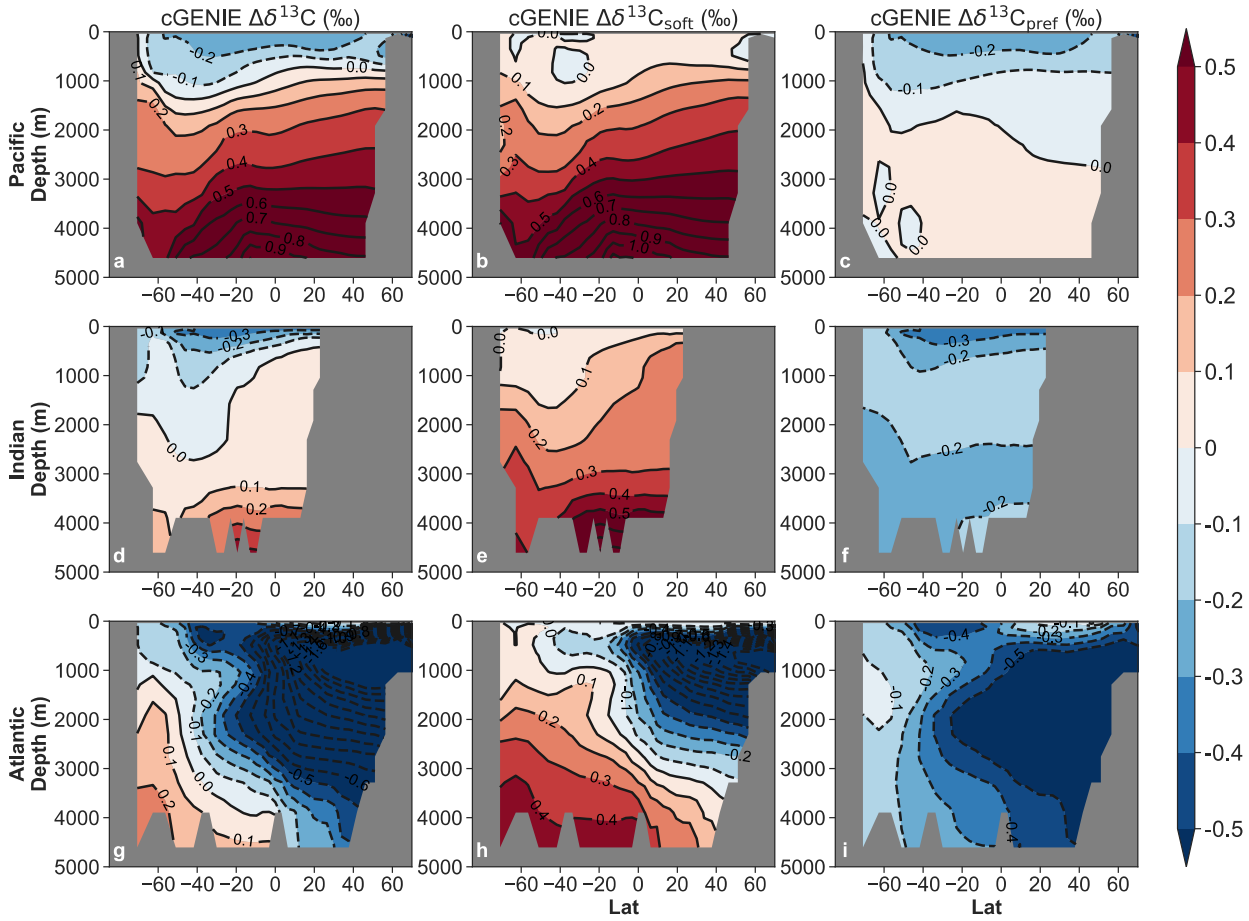

Figure 4. Ocean basin zonal mean anomalies (15ka minus 17.2ka), but for the cGENIE deglacial transient simulation. Panels are organized as in Figure 3.

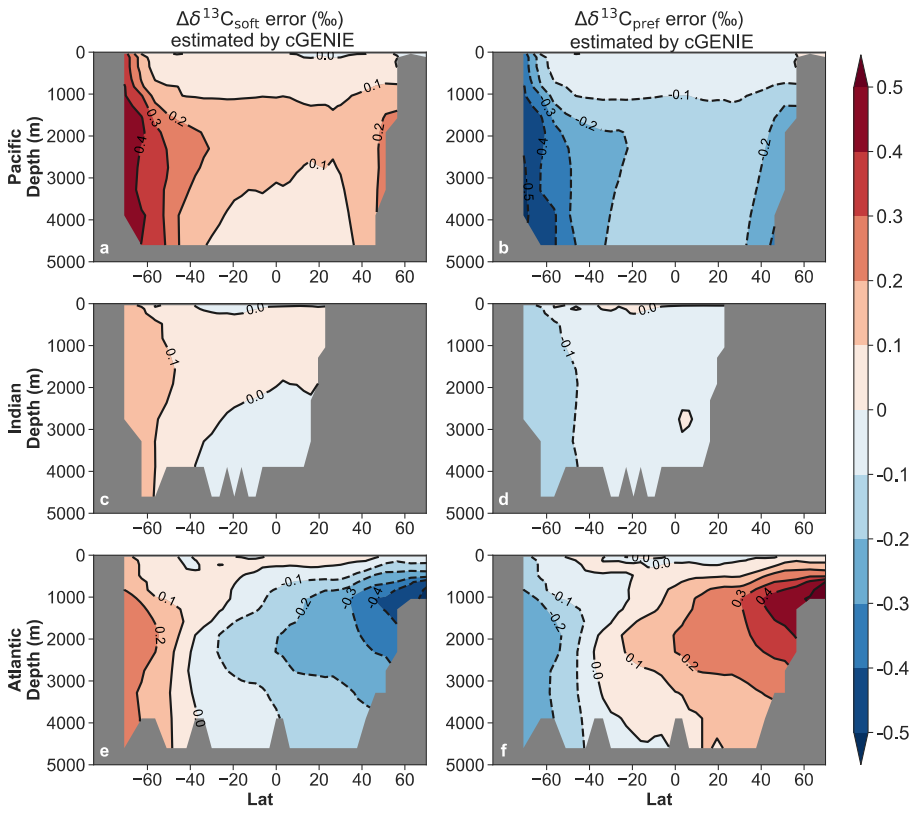

765 **Figure 5. cGENIE early deglacial transient AOU error analysis for $\Delta\delta^{13}C_{soft}$ (left column) and $\Delta\delta^{13}C_{pref}$ (right column). The anomalies are defined as 15ka minus 17.2ka. The errors are defined as AOU-based anomaly minus explicitly simulated anomaly.**

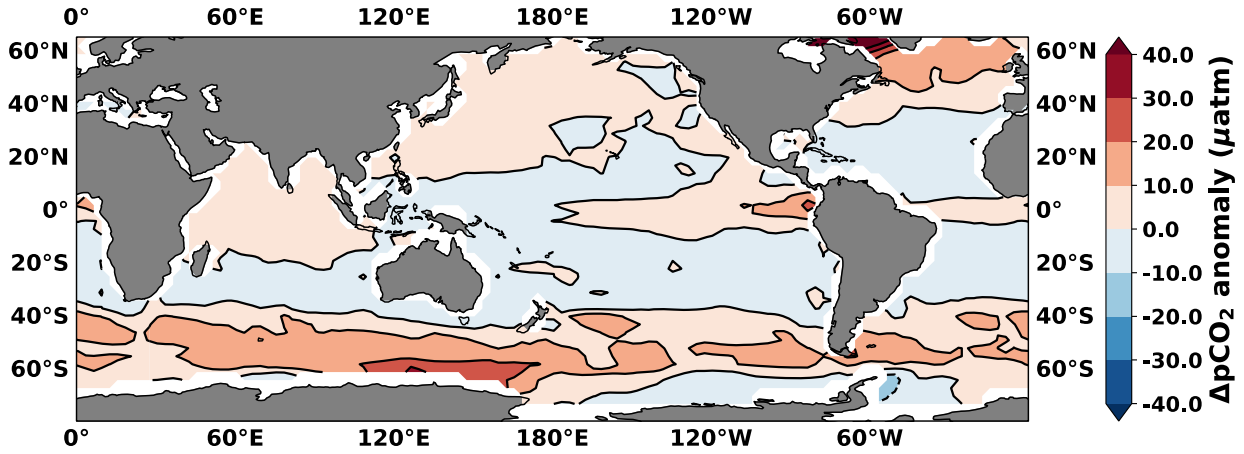

Figure 6. Changes in air-sea pCO_2 gradient (15ka minus 17.2ka) simulated by LOVECLIM.

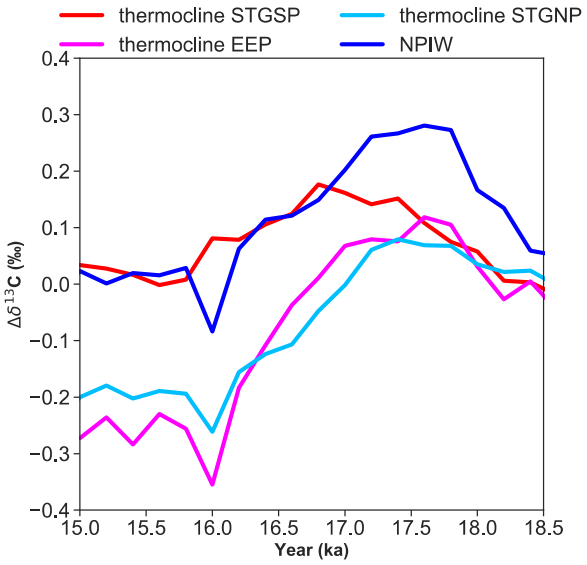

Figure 7. LOVECLIM simulated $\Delta\delta^{13}C$ in thermocline EEP (90-82°W, 5°S-5°N, 77-105m), South Pacific subtropical gyre (STGSP, 160°E- 100°W, 40-22°S, 187-400m), North Pacific subtropical gyre (STGNP, 110°E- 140°W, 22-40°N, 187-400m), NPIW (167-170°E, 54-57°N, 660m. The average of 23.8-20 ka (i.e. LGM) is used as a reference level for the $\Delta\delta^{13}C$ calculations. The interval of decreasing $\delta^{13}C$ is highlighted with a grey bar.

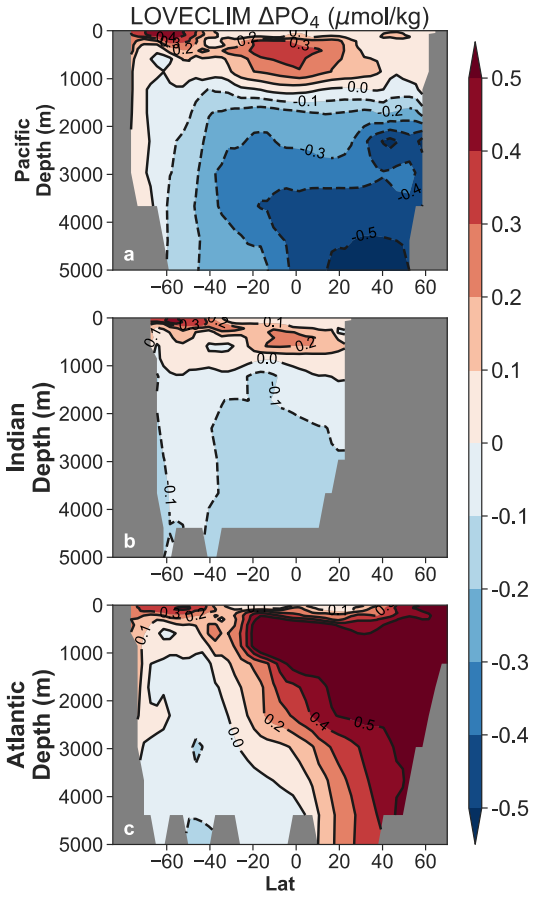

Figure 8. Ocean basin zonal mean PO_4 anomalies (15ka minus 17.2ka) as simulated in LOVECLIM.

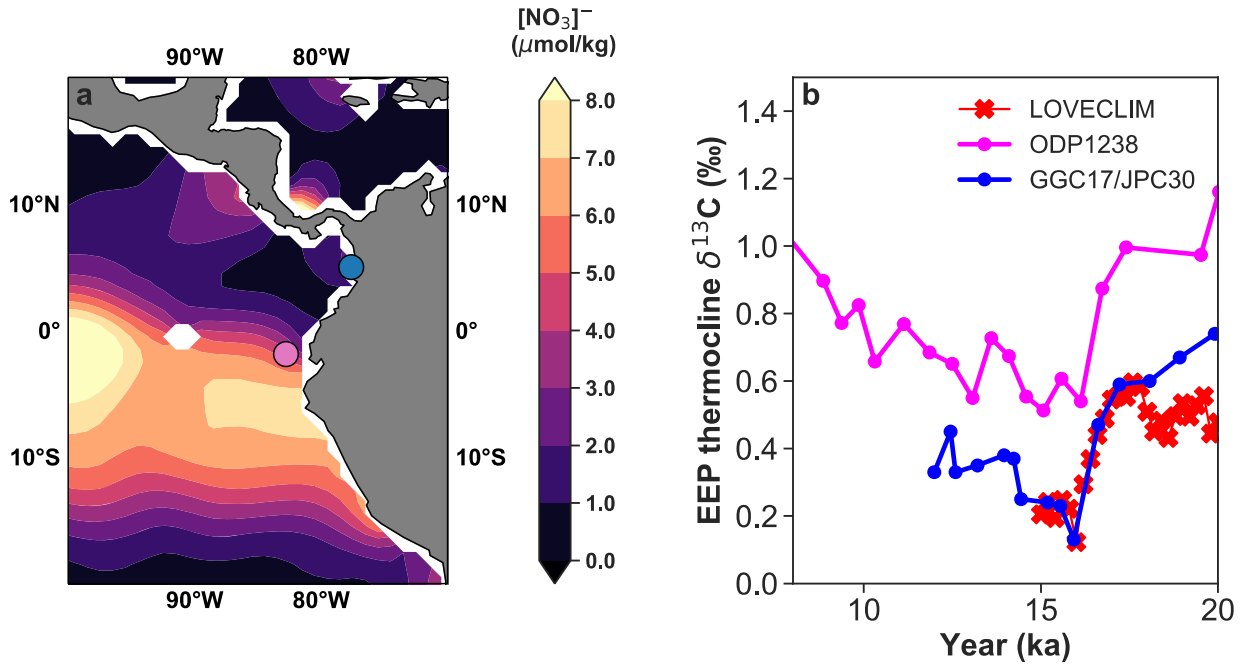

Figure 9. a): Modern sea surface nitrate concentration from the WOA 18 dataset. The site of ODP 1238 and GGC17/JPC30 are marked as a purple and blue circle, respectively. b): *Neogloboquadrina. dutertrei* (*N. dutertrei*, a shallow thermocline species) $\delta^{13}C$ data from ODP 1238 (Martínez-Botí et al., 2015), GGC17/JPC30 (Zhao and Keigwin, 2018), and LOVECLIM simulated $\delta^{13}C$ of DIC at 100m (average of 82-90°W, 5°S-5°N). The *N. dutertrei* data are corrected by -0.5‰ to normalize to $\delta^{13}C$ of DIC (Spero et al., 2003). The grey shaded bars highlight the time period we focus in this study.

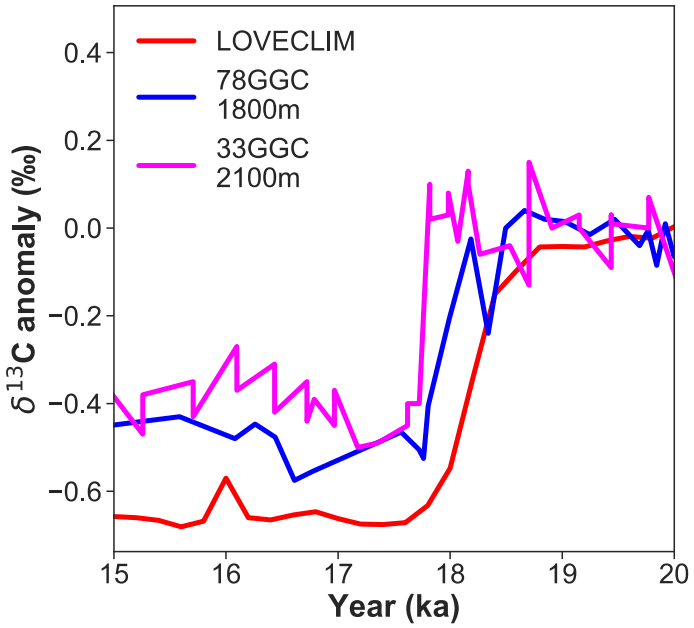

790

Figure 10. Observed $\delta^{13}C$ anomaly of 78GGC and 33GGC from the mid-depth of Brazil Margin at 27°S (Lund et al., 2015) and LOVECLIM simulated $\delta^{13}C$ anomaly at this location.

cGENIE $\delta^{13}C_{(DIC)}$ tracer decomposition and attribution error analysis

Model summary and primary tracer overview

We employ the open source intermediate complexity Earth system model cGENIE.muffin (DOI: 10.5281/zenodo.4903423) to decompose the different components comprising the stable carbon isotopic ($\delta^{13}C$) composition of dissolved inorganic carbon (DIC) in the ocean. As implemented here, cGENIE comprises: (1) a 3D ocean circulation model component configured on a 36×36 equal are grid, with 16 non-equally spaced vertical levels in the ocean, (2) a 2D energy-moisture balance model ('EMBM') component, and (3) a 2D dynamic-thermodynamic sea-ice model component. The absence of a dynamical atmospheric GCM component then requires that (fixed, annual average) 2D fields of wind stress and speed are applied, which are re-gridded from observations, plus a zonally-average profile of planetary albedo is applied. Greenhouse gas feedback on climate is implemented by applying a top of the atmosphere anomaly in radiative forcing according to the relative deviation of atmospheric CO_2 from a reference value of 278 ppm. These three individual components, their coupling, plus details of the simplified atmospheric component and associated climate feedbacks, are described in *Marsh et al.* [2011] (and references therein).

The basic physics parameter calibration of the climate model component is as per *Cao et al.* [2009]. Our implementation of cGENIE includes a relatively complete description of the cycling of carbon and oxygen in the ocean plus exchange with the atmosphere, as described in *Ridgwell et al.* [2007] and *Cao et al.* [2009]. In addition, the carbon isotopic (both $\delta^{13}C$ and radiocarbon ($\Delta^{14}C$)) composition of all the carbon pools plus associated fractionations are represented, as described in *Ridgwell et al.* [2007] with additional description and evaluation in *Kirtland Turner and Ridgwell* [2016].

In addition to basic carbon (DIC and $\delta^{13}C_{(DIC)}$), alkalinity, single nutrient (PO_4), oxygen (and sulphate) cycling in the model, we include a variety of diagnostic tracers to decompose all of the 'components' of DIC and its $\delta^{13}C$ signature. (Note that the tracer notation given here follows that of the model and associated documentation, and can deviate from that of the main paper. Equivalents are given when needed.) These explicitly simulated tracers are:

- Preformed DIC ($DIC_{(pref)}$) and preformed $\delta^{13}C_{(pref)}$.
  The values of these tracers are reset to the respective concentrations of DIC and $^{13}C_{(DIC)}$ at the ocean surface at each time-step, and thereafter are carried conservatively (no loss of gain of carbon can occur) by ocean circulation.
- Regenerated DIC from organic matter, $DIC_{(Csoft)}$ (also known as 'C_{soft}'), and its associated isotopic signature ($\delta^{13}C_{(Csoft)}$).
  In this, the value of these tracers is reset to zero at the ocean surface at each time-step. In the ocean interior, respired carbon (and for $\delta^{13}C_{(Csoft)}$, the ^{13}C component of respired carbon) associated with remineralization of both particulate and dissolved organic matter is added to the tracer field. The tracer fields are also subject to ocean circulation.
  Note that because isotopes are carried explicitly as concentrations in cGENIE (and

delta (δ) values only generated in conjunction with bulk concentrations for results output), the $\delta^{13}C_{(Csoft)}$ tracer is simulated as a concentration and exactly as per $DIC_{(Csoft)}$ and does not need to be e.g. normalized to a fractional contribution to $\delta^{13}C_{(DIC)}$ (as is required e.g. for the AOU-derived tracer, described subsequently).

- Preformed O_2 ($O_{2(pref)}$).
  The value of this tracer is reset to the concentration of dissolved O_2 at the ocean surface at each time-step, and thereafter carried conservatively (no loss of gain of dissolved oxygen can occur) by ocean circulation.
- Preformed PO_4 ($PO_{4(pref)}$).
  The value of this tracer is reset to the concentration of dissolved PO_4 at the ocean surface at each time-step, and thereafter carried conservatively (no loss of gain of dissolved phosphate can occur) by ocean circulation.

The final component of DIC – carbon released through the dissolution of $CaCO_3$ in the water column (and released from the upper sediments) – $DIC_{(CaCO3)}$ – is calculated by difference (of DIC vs. $DIC_{(pref)}$ plus $DIC_{(Csoft)}$) and is not simulated here explicitly as a separate tracer. (Ditto for $\delta^{13}C_{(CaCO3)}$.)

Steady state experiment description and basic tracer analysis

We start by performing a decomposition analysis of the carbon components, using a standard preindustrial configuration of cGENIE (*Cao et al.* [2009]) that is run for 10,000 years to steady-state. The results of this are shown broken down by basin as zonally-averaged concentrations shown in Figure S2. Notable here is the relatively insignificant contribution of $DIC_{(CaCO3)}$, particularly in the upper ca. 1000 m of the water column, where it typically contributes no more than about 10 μmol kg^{-1} DIC. (This will be important later in justifying the various assumptions inherent in the AOU-based analysis of the LOVECLIM experiment.)

In Figure S3, we show the corresponding basin zonal means of $\delta^{13}C_{(DIC)}$ simulated by cGENIE in the preindustrial ocean, together with the 3 components that contribute to the net distribution. Notable again here is the weak contribution that can be ascribed to the dissolution of $CaCO_3$. Indeed, in the upper ca. 1000 m of the water column, the (positive) contribution of $\delta^{13}C_{(CaCO3)}$ is generally less than about 0.05‰, compared to a contribution from $\delta^{13}C_{(Csoft)}$ that can exceed (in magnitude) -2.0‰ and to a $\delta^{13}C_{(pref)}$ contribution lying between ca. 1.5 and 2.5‰. Note the different (to $\delta^{13}C_{(Csoft)}$) color scale for $\delta^{13}C_{(CaCO3)}$ and that the surface (and convected-to-depth in the North Atlantic) apparent high values (purple colors) are an artifact of the differencing of DIC and $^{13}C_{(DIC)}$ concentrations used in calculating $\delta^{13}C_{(CaCO3)}$ (i.e. at close-to-zero values for $DIC_{(CaCO3)}$ spurious apparent isotopic values can arise).

In a final, simple numerical check of this diagnostic tracer scheme (not shown), we re-run the 10,000 year preindustrial experiment but with the production of $CaCO_3$ at the ocean surface disabled, i.e. in the complete absence of any $\delta^{13}C_{(CaCO3)}$ component to $\delta^{13}C_{(DIC)}$. From this we confirm, as expected, that $DIC = DIC_{(pref)} + DIC_{(Csoft)}$, and $\delta^{13}C_{(DIC)} = \delta^{13}C_{(pref)} + \delta^{13}C_{(Csoft)}$ to within 0.03‰. That this error is not zero to within numerical precision, is due to the specific numerical scheme and implementation of the preformed and regenerated tracers in cGENIE. As described in the main text, for the preformed tracers, an anomaly is applied at the ocean surface at each time-step, equal to the difference between the current bulk tracer value and the preformed

tracer value (as opposed to simply directly setting the values equal in the code). Because in the numerical scheme, all fluxes, including those induced by ocean circulation and any preformed tracer anomalies, are calculated simultaneously and only summed and applied to update the tracer concentration field at the very end of the model time-step, preformed tracer concentrations at the ocean surface and at the end of the time-step, never exactly equal those of the bulk tracer. The maximum error (ca. -0.03‰) occurs at the surface of the Southern Ocean as a result of the energetic ocean transport environment (principally, convection) there. This error is propagated throughout the ocean, creating a mean ocean net error of -0.012‰ in the diagnostic tracer scheme.

Summary of calculated 'derived' tracers

Although LOVECLIM is able to simulate preformed PO_4, P_{pre} and hence calculate regenerated PO_4 by differencing with (total) [PO_4], and then to C_{soft} by scaling with a P:C ratio – see Menviel et al. [2015]), LOVECLIM was not run with this tracer included in the published deglacial experiment used in this study. Instead, C_{soft} in LOVECLIM must be estimated from apparent oxygen utilization (AOU) (for example, as applied to output from the Bern3D model in Menviel et al. [2015]). To quantify the errors inherent in this approach, we calculate a number of derived tracer fields based on the primary (simulated) ones:

1. $O_{2(sat)}$ – O_2 solubility at every ocean grid point using ambient temperature and salinity values (plus density, ρ). For this, we calculate the solubility coefficient (α, mol kg^{-1} atm^{-1}) for O_2 following Wanninkhof (1992) and using the coefficients from *Millero and Sohn* [1992], and assume an atmospheric partial pressure for oxygen (pO_2) of 0.2096 atm:
   $O_{2(sat)} = \rho \times \alpha \times pO_2$
   (This diagnostic employs the exact same calculation as used 'normally' in cGENIE for simulating air-sea gas exchange (Ridgwell et al., 2007).)
2. AOU – calculated as the difference between $O_{2(sat)}$ and the actual model simulated tracer field of [O_2]:
   $O_{2(AOU)} = O_{2(sat)} - [O_2]$
3. AOU-P – regenerated PO_4 – estimated from AOU divided by the assumed cGENIE O_2:P Redfield ratio of (-)138:1:
   $P_{(AOU)} = O_{2(AOU)} / 138$
   Note that for the purposes of this analysis, we ignore complications caused by the occurrence of sulphate reduction in oxygen minimum zones, meaning that locally, there will be a 'missing' fraction of regenerated phosphate that is not associated with AOU. For reference, the global oxygen consumption associated with particulate organic carbon oxidation in the preindustrial experiment is 608 Tmol O_2 yr^{-1}, while (in the absence of nitrate reduction) the global rate of SO_4^{2-} consumption is 29 Tmol SO_4^{2-} yr^{-1} (equivalent to 58 Tmol O_2 yr^{-1}). However, this does not equate to a ~10% global error in estimating AOU-P, because the re-oxidation of H_2S consumes dissolved oxygen, closing the AOU budget. Rather, the impact of not accounting for SO_4^{2-}/H_2S transformations will be a pattern of positive and negative error in estimating regenerated PO_4 from AOU.

4. AOU-DIC – DIC regenerated from organic matter – estimated from AOU-P multiplied by the assumed cGENIE P:C Redfield ratio of 1:106:
   $DIC_{(AOU)} = 106 \times P_{(AOU)}$
   This is an estimate of C_{soft}.
5. AOU-$\delta^{13}C$ – the $\delta^{13}C$ contribution of DIC from regenerated from organic matter – estimated by weighting the $\delta^{13}C$ of POC exported from the overlying ocean surface ($\delta^{13}C_{(Corg)}$) by the fractional contribution of AOU-DIC to (total) DIC:
   $\delta^{13}C_{(AOU)} = \delta^{13}C_{(Corg)} \times DIC_{(AOU)}/DIC$
   This is an estimate of $\delta^{13}C_{(Csoft)}$.
6. C_{soft}-$\delta^{13}C$ – the $\delta^{13}C$ contribution of DIC from regenerated from organic matter – estimated by weighting the $\delta^{13}C$ of POC exported from the overlying ocean surface by the fractional contribution of C_{soft} to (total) DIC:
   $\delta^{13}C_{(Csoft)'} = \delta^{13}C_{(Corg)} \times DIC_{(Csoft)}/DIC$
   This is an alternative estimate of $\delta^{13}C_{(Csoft)}$ that is independent of the assumptions inherent in AOU. It also acts as a test of the assumption that one can tag regenerated carbon ($DIC_{(Csoft)}$) with the isotopic signature of POC exported from the overlying ocean in order to estimate regenerated $\delta^{13}C$. Note that this post-processed diagnostic ($\delta^{13}C_{(Corg)}$-prime) is distinct from the explicitly simulated $\delta^{13}C_{(Csoft)}$ tracer (see description of primary tracers).

For completeness, we also simulate but do not report, $P_{(pref)}$, and from this derive regenerated P ($P_{(Csoft)}$) and hence can obtain a second alternative estimate of the $\delta^{13}C$ contribution of DIC from regenerated organic matter ($\delta^{13}C_{(Csoft)''}$).

All outputs are calculated on the basis of annual mean values of the 3D ocean tracer fields.

Steady state analysis of the errors inherent in estimating C_{soft}-$\delta^{13}C$

We start our derived tracer analysis by illustrating the errors inherent in AOU itself. As is widely appreciated, AOU overestimates the consumption of oxygen through respiration as a consequence of incomplete equilibrium occurring between the ocean surface and overlying atmosphere which causes $O_{2(sat)}$ to be an overestimation of real ocean oxygenation. There is also an estimation error due to the non-linear solubility of oxygen, which follows a quasi-exponential decay with increasing temperature. This results in an *underestimate* of AOU, because $O_{2(sat)}$ is underestimated when calculated from the ambient (linear mixing) temperature of parcels of water derived from sources equilibrated at 2 (or more) different sea surface temperatures. Figure S4 shows the difference between AOU and 'true' oxygen utilization (TOA), with the latter calculated as the difference between preformed [O_2] ($O_{2(pref)}$) and simulated ambient [O_2]. From this it is clear that the disequilibrium error dominates, with the surface overestimate in AOU and its propagation into the ocean interior being particularly pronounced at high southern latitudes. While cGENIE calculates an AOU error about 30% smaller than originally reported by *Ito et al.* [2004] using the MIT OGCM, our results fall between the range of the different (higher resolution) models presented by *Duteil et al.* [2013]. The zonal patterns calculated by cGENIE (Figure S4) are also similar to the Atlantic and Pacific sections presented in both papers (*Ito et al.* [2004], *Duteil et al.* [2013]).

Converting AOU to AOU-C (the AOU-derived estimate of respired carbon – see above), translates to an error (overestimate) in C_{soft} of around 30 μmol kg^{-1}, which dominates all of the deep Pacific and Indian Ocean below about 1000 m (Figure S6). (In cGENIE, the North Atlantic Ocean surface is closer to equilibrium and full oxygenation and hence creates a plume of relatively low DIC error waters along the path of North Atlantic deep water.) However, we find that the $\delta^{13}C$ error – the difference between explicitly simulated $\delta^{13}C_{(Csoft)}$ and the AOU-based estimation (AOU-$\delta^{13}C$) – deviates noticeably from the pattern of the DIC error (Figure S5, 2nd row down). Specifically: while the largest error in $\delta^{13}C_{(Csoft)}$ is indeed found throughout the water column in the Southern Ocean, following the error in AOU and the C_{soft} field derived from this, the mid and low latitudes are characterized by much reduced error in $\delta^{13}C_{(Csoft)}$ and deviate from the pattern of DIC error (top row). Somewhat enigmatically, a prominent $\delta^{13}C_{(Csoft)}$ error maximum is also found throughout much of the water column in the North Pacific (but not at the northern-most end of the Indian Ocean). We resolve this by differencing AOU-$\delta^{13}C$ (#5) and C_{soft}-$\delta^{13}C$ (#6), whereby the error associated with assuming a fixed value field of $\delta^{13}C_{(POC)}$ cancels out, leaving only the error in deriving C_{soft} from AOU. This $\delta^{13}C$ error field (Figure S5, 2nd row from bottom) now visually correlates much more closely with the AOU DIC error field (top row). The 2nd component to the total AOU based C_{soft}-$\delta^{13}C$ error can be calculated as the difference between 'true' (explicitly simulated) C_{soft}-$\delta^{13}C$, and C_{soft}-$\delta^{13}C$ estimated from $DIC_{(Csoft)}$ together with $\delta^{13}C_{(POC)}$ (#6). This is shown in the final row of Figure S5. Here, it can be seen that a significant positive error arises at mid-to-low latitude in the ocean subsurface.

What this analysis reveals is a flaw in how C_{soft}-$\delta^{13}C$ is being estimated by convoluting a field of exported $\delta^{13}C_{(POC)}$ with C_{soft}. The 'true' C_{soft}-$\delta^{13}C$ tracer field is not only a product of local DIC release (from organic carbon remineralization) with its associated local isotopic value ($\delta^{13}C_{(POC)}$), but also how the composition of a parcel of water is transformed as it moves through the deep ocean. The C_{soft}-$\delta^{13}C$ tracer field is hence an integrated history of isotopic remineralization, just as C_{soft} is an integrated history of bulk carbon remineralization. Importantly, in the real ocean, and to some extent simulated in many models including cGENIE, $\delta^{13}C_{(POC)}$ varies significantly spatially: from values less than (more negative) than -30‰ towards the poles, to more (less negative) than -20‰ at the equator. Hence, tagging an equatorial subsurface parcel of water with an equatorial-only $\delta^{13}C_{(POC)}$ value omits the history of that water mass that will have started at high latitudes where initially it receives a much more isotopically depleted remineralized carbon input. Notably and rather more by luck than design, models either assuming a fixed fractionation of POC $\delta^{13}C$ vs. DIC $\delta^{13}C$, or like LOVECLIM, otherwise producing a relatively small pole-to-equator gradient in POC $\delta^{13}C$, will be subject to only a small associated error in convoluting exported $\delta^{13}C_{(POC)}$ with C_{soft} (and leaving the related error related to the AOU approximation dominant everywhere).

Transient* C_{soft}-$\delta^{13}C$ *error analysis

So far, we have only considered only a steady-state situation and the question arises: what happens during climate and carbon cycle change – do the error fields change and relatively by how much? For the final part of our diagnostic tracer framework analysis we turn to a simple transient simulation. For this, we take the same model preindustrial steady state, but apply (and hold) a radiative forcing at the top of the atmosphere equivalent to a doubling of

atmospheric *p*CO2 (to 556 ppm). The actual value of pCO_2 simulated in the model is free to vary in response to the applied surface warming, but this does not affect the imposed radiative forcing. (Note that no injection of carbon to the atmosphere is used to induce the warming, and both bulk and ^{13}C carbon inventories are conserved between ocean+atmosphere as compared to the preindustrial spin-up.) The evolution over 2000 years of key global mean atmospheric and climate variables, along with mean ocean $\delta^{13}C_{(DIC)}$, $\delta^{13}C_{(pref)}$, and $\delta^{13}C_{(Csoft)}$, are shown in Figure S6. We pick 2 contrasting time-horizons to focus our final tracer analysis on: (1) 200 years, which corresponds in terms of time, to the 'rapid' interval from 16.3-16.1 ka of atmospheric $\delta^{13}C$ decline recorded in ice-cores (and coincidently corresponds to the interval of most rapid $\delta^{13}C_{(pref)}$ and $\delta^{13}C_{(Csoft)}$ change in our simple experiment), and (2) 2000 years, which approximately corresponds to the overall 17.2 to 15 ka early deglaciation interval. Note that imposing enhanced radiative forcing on a preindustrial state is not meant to replicate deglaciation. Rather, we deliberately create as simple a transient climate and carbon cycle change as possible for the purpose of assessing non steady-state diagnostic tracer behavior. However, although the warming approximately corresponds in overall magnitude to that associated with deglaciation and is additionally associated with reorganization of the Atlantic Meridional Overturning Circulation, it should also be noted that this idealized instantaneous-perturbation transient experiment is distinct from the deglacial-like experiment described and analyzed in the main text.

Figure S7 shows the change in $\delta^{13}C_{(DIC)}$ as compared to a control (continuing preindustrial) experiment for year 200 (top) and 2000 (2^{nd}-from-top row). In this specific idealized cGENIE model experiment, the patterns of change in $\delta^{13}C_{(DIC)}$ are dominated by changes in nutrient re-supply to the ocean surface, and hence the strength of the biological export from the surface and organic matter remineralization in the ocean interior – all in turn reflected in changes in $\delta^{13}C_{(Csoft)}$ (not shown). In contrast, changes in $\delta^{13}C_{(pref)}$ (not shown) are largely confined to the upper ca. 1000 m as a result of CO_2 outgassing as the ocean warms. We also calculate how the error in $\delta^{13}C_{(Csoft)}$ as estimated from AOU changes – shown in the 2^{nd}-from-bottom and bottom rows of Figure S7 for year 200, and 2000, respectively. We find that the isotopic error across the uppermost ca. 500 m in the model hardly changes as compared to the control (the close-to-zero anomaly values in Figure S7) and after 2000 years, as the system starts to re-establish a steady state, the spatial distribution of the error anomaly largely follows that of the steady state AUO error (SI Figure 4).

cGENIE* C_{soft}-$\delta^{13}C$ *analysis summary

Relevant to the LOVECLIM model analysis conducted in the paper, we can conclude the following from the above experiments and analysis:

i. With a relatively minimal latitudinal gradient in the $\delta^{13}C$ signature of exported POC in LOVECLIM, the error in estimating $\delta^{13}C_{(Csoft)}$ and hence the relative contribution of $\delta^{13}C_{(Csoft)}$ vs. $\delta^{13}C_{(pref)}$ to a given simulated $\delta^{13}C_{(DIC)}$ change in LOVECLIM, will be dominated primarily by the error in estimating C_{soft} from AOU. (cGENIE, in contrast, sees approximately equivalent-in-magnitude error terms due to both error sources throughout the low and mid latitudes – Figure S5.)

ii. At least in the context of the idealized transient experiment tested here, the AOU-induced $\delta^{13}C_{(Csoft)}$ error is almost invariant throughout the uppermost ca. 500 m of the ocean (Figure S7). This is likely simply because the AOU error in $\delta^{13}C_{(Csoft)}$ is close to zero in this region of the ocean to start with (Figure S5) and that AOU provides a relatively reliable means of estimating C_{soft} here. The important point is that this is close to the depth range where planktic and (most) shallow benthic foraminifera are sampling the isotopic composition of DIC.

References:

Cao, L., Eby, M., Ridgwell, A., Caldeira, K., Archer, D., Ishida, A., Joos, F., Matsumoto, K., Mikolajewicz, U., Mouchet, A., Orr, J. C., Plattner, G.-K., Schlitzer, R., Tokos, K., Totterdell, I., Tschumi, T., Yamanaka, Y., and Yool, A.: The role of ocean transport in the uptake of anthropogenic CO_2, 6, 375–390, https://doi.org/10.5194/bg-6-375-2009, 2009.

Kirtland Turner, S. and Ridgwell, A.: Development of a novel empirical framework for interpreting geological carbon isotope excursions, with implications for the rate of carbon injection across the PETM, Earth and Planetary Science Letters, 435, 1–13, https://doi.org/10.1016/j.epsl.2015.11.027, 2016.

Marsh, R., Müller, S. A., Yool, A., and Edwards, N. R.: Incorporation of the C-GOLDSTEIN efficient climate model into the GENIE framework: "eb_go_gs" configurations of GENIE, Geosci. Model Dev., 4, 957–992, https://doi.org/10.5194/gmd-4-957-2011, 2011.

Ridgwell, A., Hargreaves, J. C., Edwards, N. R., Annan, J. D., Lenton, T. M., Marsh, R., Yool, A., and Watson, A.: Marine geochemical data assimilation in an efficient Earth System Model of global biogeochemical cycling, 4, 87–104, 2007.

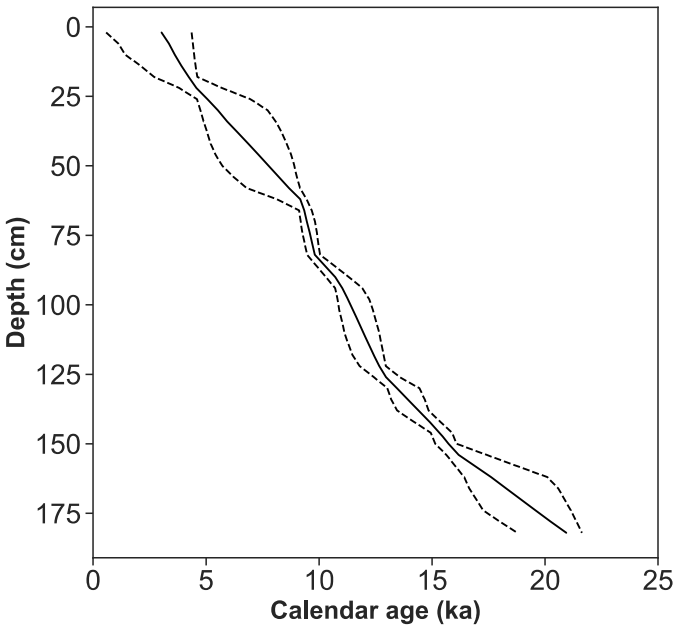

Figure S1. Age model of GeoB17402-2. The dash lines represent 2.5% and 97.5% quantile of the assigned ages.

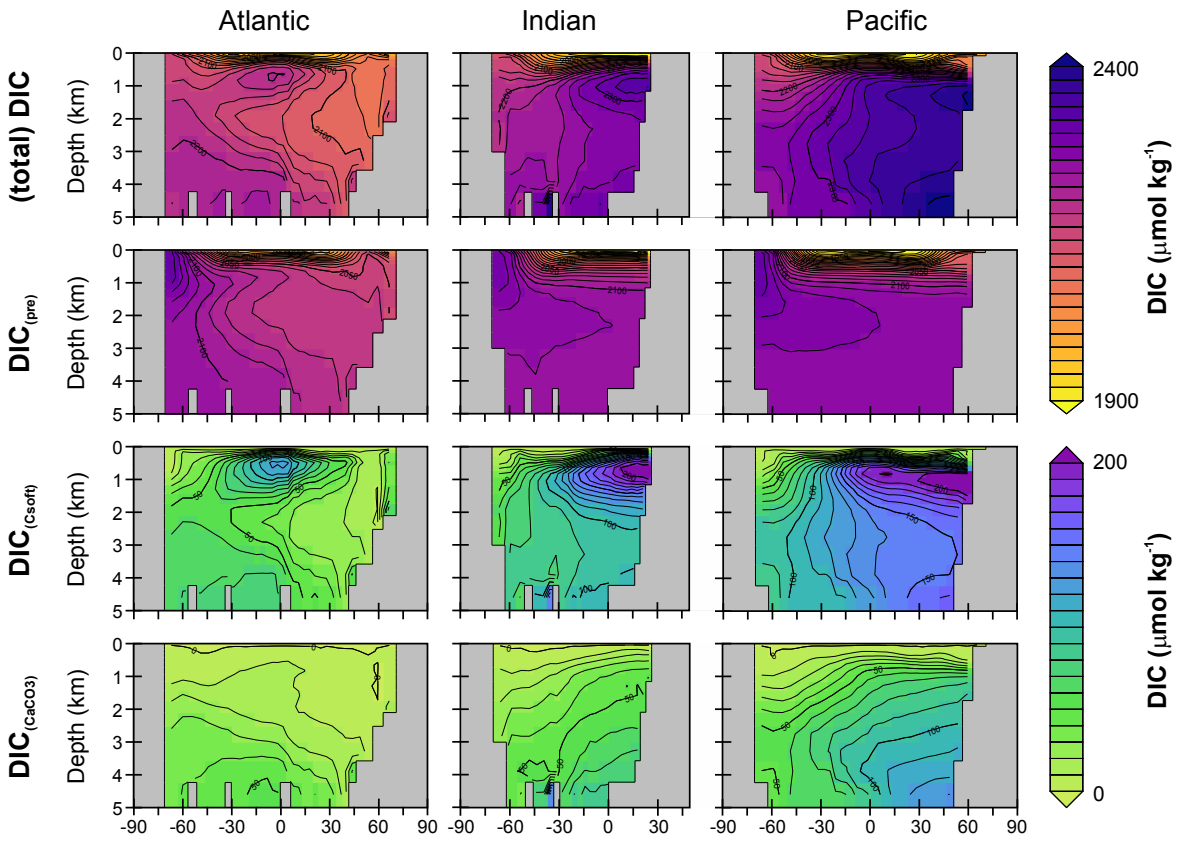

Figure S2. cGENIE preindustrial steady state, mean annual zonally averaged, DIC, DIC_{pref}, DIC_{soft} and DIC_{caco3} distributions.

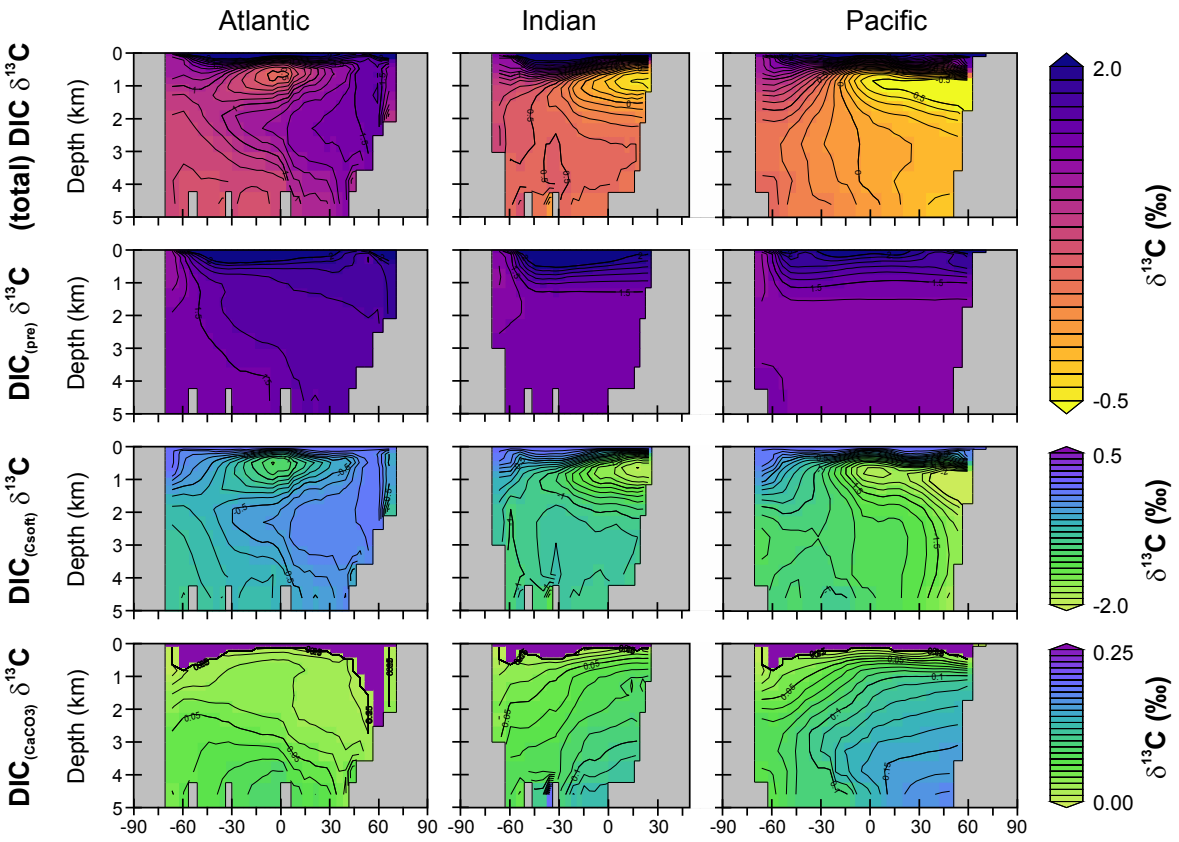

Figure S3. cGENIE preindustrial steady state, mean annual zonally averaged, distributions of the $\delta^{13}C$ of DIC, DIC_{pref}, DIC_{soft} and DIC_{caco3}.

290

Figure S4. cGENIE preindustrial steady state AOU error analysis.

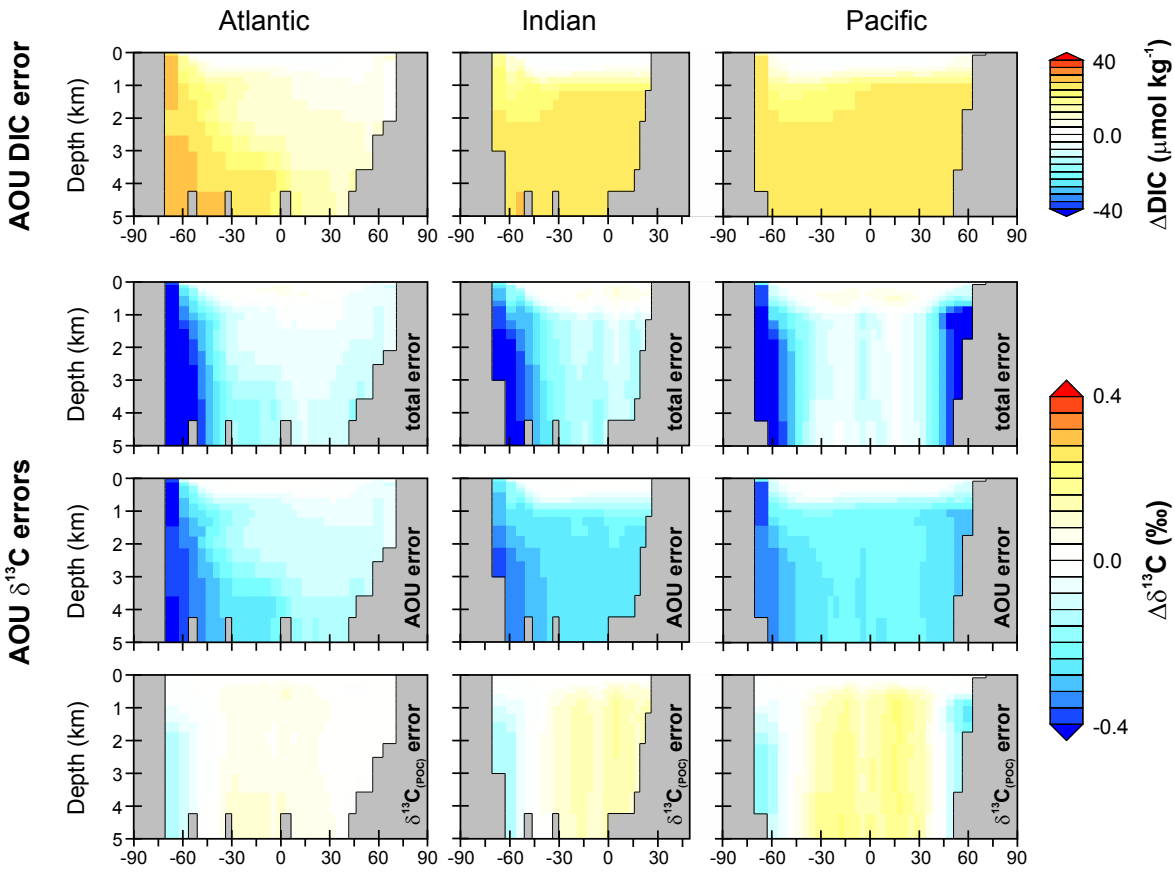

295

Figure S5. cGENIE preindustrial steady state AOU-based DIC and $\delta^{13}C$ error analysis.

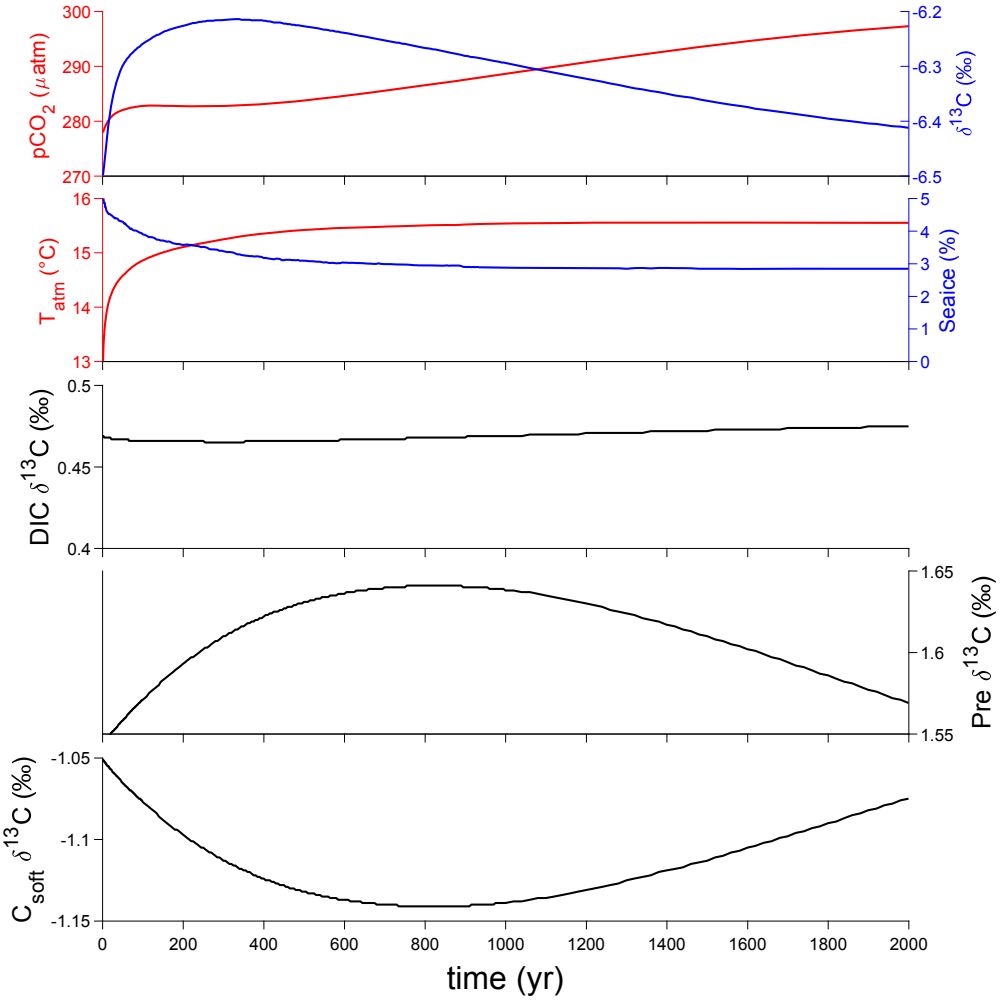

Figure S6. Time-series of cGENIE 2000-year idealized transient experiment.

300

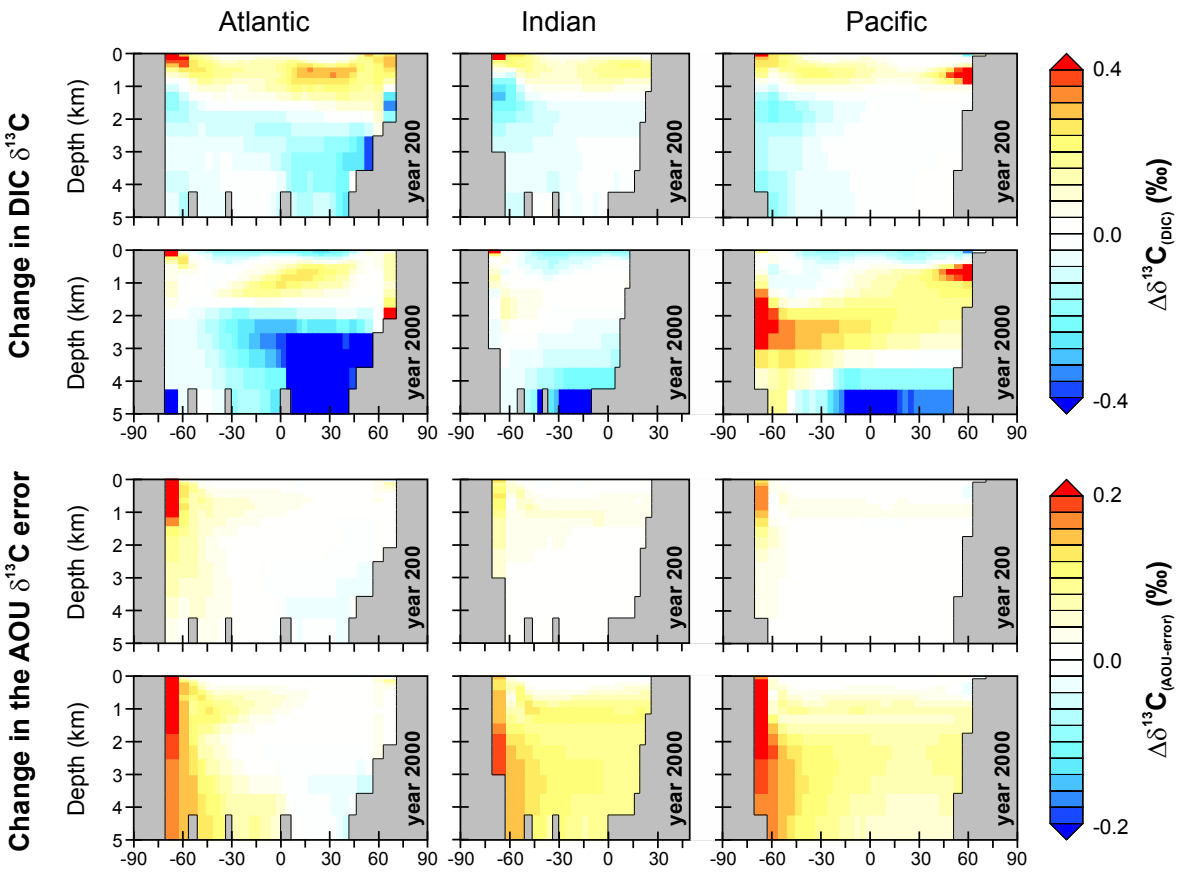

Figure S7. cGENIE 2000-year idealized transient experiment AOU error analysis.

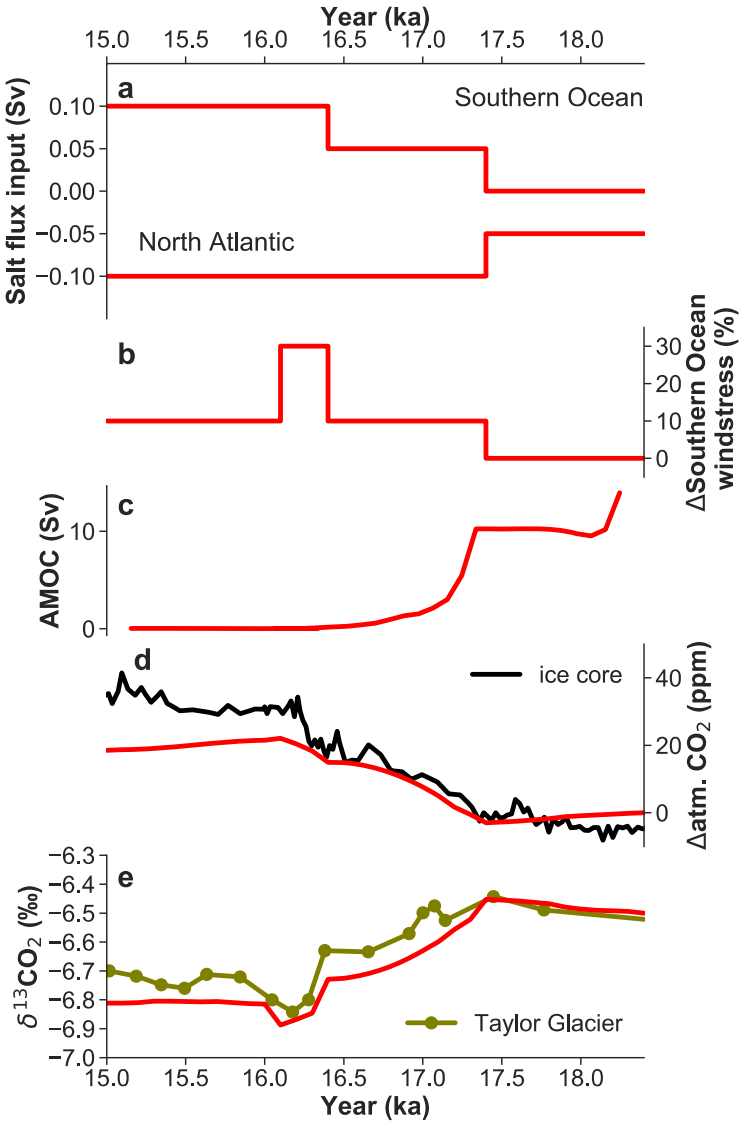

Figure S7. Forcing and atmospheric response in the cGENIE deglacial transient experiment.

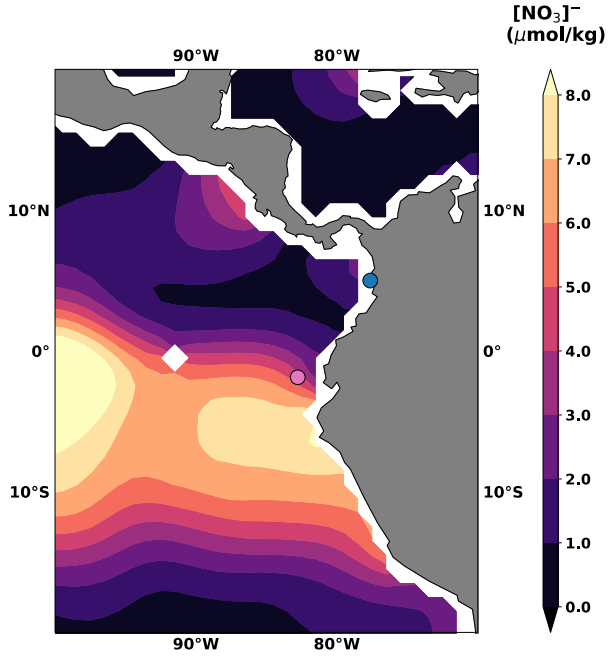

Figure S8. Modern sea surface nitrate concentration from the WOCE13 dataset. The site of ODP 1238 and GGC17/JPC30 are marked as a purple and blue circle, respectively.

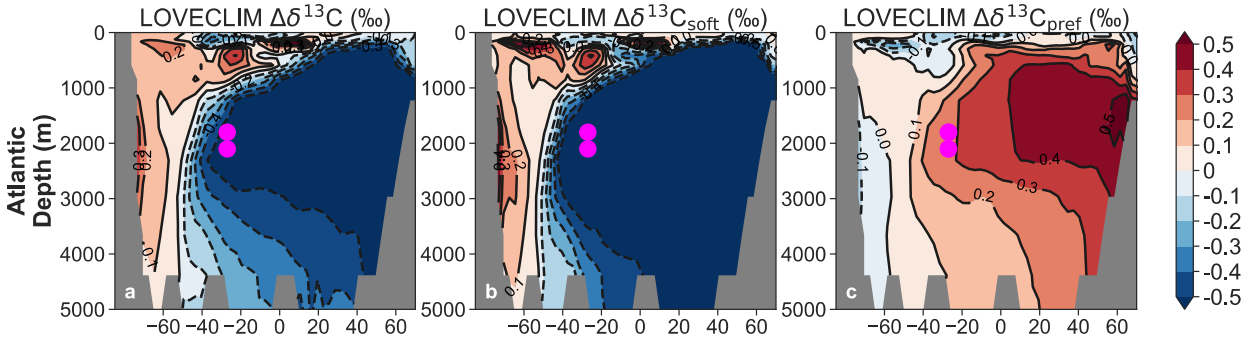

Figure S9. Atlantic zonal mean anomaly (60°W-10°W) in LOVECLIM. The magenta circles mark the 78GGC and the 33GGC site. All anomalies are defined as 17.2ka minus 19ka.